A&A 546, A63 (2012)
DOI: 10.1051/0004-6361/201118410

Astronomy & Astrophysics

Astrometric confirmation of young low-mass binaries and multiple systems in the Chamaeleon star-forming regions⋆,⋆⋆

N. Vogt[1,2], T. O. B. Schmidt[3], R. Neuhäuser[3], A. Bedalov[4], T. Roell[3], A. Seifahrt[5,6], and M. Mugrauer[3]

[1] Departamento de Física y Astronomía, Universidad de Valparaíso, Avenida Gran Bretaña 1111, Valparaíso, Chile
e-mail: Nikolaus.Vogt@uv.cl
[2] Instituto de Astronomía, Universidad Catolica del Norte, Avda. Angamos 0610, Antofagasta, Chile
[3] Astrophysikalisches Institut und Universitäts-Sternwarte, Universität Jena, Schillergäßchen 2-3, 07745 Jena, Germany
[4] Faculty of Natural Sciences, University of Split, Teslina 12, 21000 Split, Croatia
[5] Department of Physics, University of California, Davis, CA 95616, USA
[6] Department of Astronomy and Astrophysics, University of Chicago, Chicago, IL 60637, USA

Received 7 November 2011 / Accepted 13 March 2012

ABSTRACT

Context. The star-forming regions in Chamaeleon (Cha) are one of the nearest (distance ~ 165 pc) and youngest (age ~ 2 Myr) conglomerates of recently formed stars and the ideal target for population studies of star formation.
Aims. We investigate a total of 16 Cha targets that have been suggested, but not confirmed, to be binaries or multiple systems in previous literature.
Methods. We used the adaptive optics instrument Naos-Conica (NACO) at the Very Large Telescope Unit Telescope (UT) 4 / YEPUN of the Paranal Observatory, at 2–5 different epochs, in order to obtain relative and absolute astrometric measurements, as well as differential photometry in the J, H, and K band. On the basis of known proper motions and these observations, we analyse the astrometric results in our proper motion diagram (PMD: angular separation / position angle versus time), to eliminate possible (non-moving) background stars, establish co-moving binaries and multiples, and search for curvature as indications for orbital motion.
Results. All previously suggested close components are co-moving and no background stars are found. The angular separations range between 0.07 and 9 arcsec, corresponding to projected distances between the components of 6–845 AU. Thirteen stars are at least binaries and the remaining three (RX J0919.4-7738, RX J0952.7-7933, VW Cha) are confirmed high-order multiple systems with up to four components. In 13 cases, we found significant slopes in the PMDs, which are compatible with orbital motion whose periods (estimated from the observed gradients in the position angles) range from 60 to 550 years. However, in only four cases there are indications of a curved orbit, the ultimate proof of a gravitational bond.
Conclusions. A statistical study based on the 2MASS catalogue confirms the high probability of all 16 stellar systems being gravitationally bound. Most of the secondary components are well above the mass limit of hydrogen burning stars (0.08 $M_\odot$), and have masses twice as high as this value or more. Massive primary components appear to avoid the simultaneous formation of equal-mass secondary components, while extremely low-mass secondary components are hard to find for both high and low mass primaries owing to the much higher dynamic range and the faintness of the secondaries.

Key words. stars: imaging – stars: pre-main sequence – binaries: general – binaries: close – astrometry – infrared: stars

1. Introduction

One of the nearest dark cloud groups to the Sun can be found in the southern constellation Chamaeleon, at a distance of 165 ± 30 pc (based on the data of Bertout et al. 1999; and Whittet et al. 1997). There are strong indications of recent star formation within these clouds: many newborn stars have been historically detected according to their variability and Hα emission. Their observed location in the Hertzsprung-Russell diagram implies, according to the evolutionary models of Chabrier et al. (2000) and Baraffe et al. (2003), that Cha I has a mean age of ~2×10^6 years (Luhman 2008). The stellar density within this region is rather low, but contains a large number of low mass stars. Since the Chamaeleon association is nearby and well-isolated from other young stellar populations it is an excellent target for studies of low-mass star formation. For a review about this region we refer to Luhman (2008).

Our main interests are the frequency and distribution of young binaries and multiple systems, with emphasis on the occurrence of components near the stellar mass limit (0.08 $M_\odot$), and of brown dwarfs or planets. For this purpose, we carried out an extensive observational campaign to search for possible companion objects of the most certain members of the Chamaeleon association with well-known proper motions. We obtained direct imaging of a total of 51 Cha association member stars with the European Southern Observatory (ESO) Very Large Telescope (VLT) instrument Naos-Conica (NACO, Lenzen et al. 2003; Rousset et al. 2003), in the near-infrared (J, H, and Ks) to carry out high precision astrometry and photometry of them and their nearby candidate companions. In some cases, follow-up spectroscopic observations could be obtained, as for Cha Hα 2 (Schmidt et al. 2008b) and CT Cha (Schmidt et al. 2008a). The

⋆ Based on observations made with ESO telescopes at the Paranal Observatory under program IDs 076.C-0292(A), 078.C-0535(A), 080.C-0424(A), 082.C-0489(A), 084.C-0364(B), 086.C-0638(A) & 086.C-0600(B), the Hubble Space Telescope under program ID GO-8716 and data obtained from the ESO/ST-ECF Science Archive Facility from the Paranal Observatory under program IDs 075.C-0042(A), 076.C-0579(A), 278.C-5070(A) and from the Hubble Space Telescope under programme IDs SNAP-7387, GO-11164.
⋆⋆ Appendix A is available in electronic form at http://www.aanda.org

Table 1. Observed objects in Chamaeleon.

Object[a]	RA [h m s][a,b]	Dec [° ′ ″][a,b]	System architecture[c]	Bin. Ref.	Spectral-types	SpT Ref.	Dist. [pc]	Dist. Ref.	2MASS K [mag][d]	Backg.[e] density
RX J0915.5-7609	09 15 29.12	–76 08 47.2	**	1	K7+?	2	168	3	8.488	0.135
RX J0919.4-7738	09 19 24.96	–77 38 37.0	SB2+**	4, 2, 1	G7+?+K0+?	5	57	6	6.780	0.137
RX J0935.0-7804	09 34 56.04	–78 04 19.4	**	1	M2+?	2	168	3	8.889	0.132
RX J0952.7-7933	09 53 13.74	–79 33 28.5	*+SB2	2, 1	F6?+F6+F6?	2	170?	7	7.994	0.122
RX J1014.2-7636	10 14 08.07	–76 36 32.8	**	1	M3+?	2	165?		8.874	0.154
SZ Cha	10 58 16.77	–77 17 17.1	SB?+*+w*	8, 9	K0+M5+?	9, 10	165	Cha I	7.758	0.144
Ced 110 IRS 2	11 06 15.41	–77 21 57.0	**+w*	10, 11	G5+?+?	12	165	Cha I	6.419	0.056
Cha Hα 2	11 07 42.46	–77 33 59.4	**	13, 14	M6+M6?	15	165	Cha I	10.675	0.062
VW Cha	11 08 01.49	–77 42 28.9	SB?+**+w*	16, 17	K6+K7+?+M2.5	18	165	Cha I	6.962	0.088
RX J1109.4-7627	11 09 17.70	–76 27 57.8	**	19, 20	K7+?	2	165	Cha I	8.701	0.141
HD 97300	11 09 50.02	–76 36 47.7	**	8	B9+?	21	179	6	7.149	0.098
WX Cha	11 09 58.74	–77 37 08.9	**	8	K0-M1.25+?	12	165	Cha I	7.970	0.096
WY Cha	11 10 07.05	–76 29 37.7	**+w*	20, 10	K2-M0+?+?	12	165	Cha I	8.451	0.127
HJM C 7-11	11 10 38.02	–77 32 39.9	SB?+*+w*	8, 22	K3+?+?	2	165	Cha I	8.277	0.107
Sz 41	11 12 24.42	–76 37 06.4	SB?+*+w*	23	K4+?+G8	2, 24	165	Cha I	7.999	0.166
HM Anon	11 12 42.69	–77 22 23.1	**	8	G8+?	25	165	Cha I	7.880	0.124

Notes. [(a)] Taken from the SIMBAD database (Wenger et al. 2007). [(b)] International Celestial Reference System (ICRS) coordinates (epoch = J2000). [(c)] Previously known and supposed multiplicity of the objects: *: star, **: binary, SB: spectroscopic binary, SB2: double-lined spectroscopic binary, w*: wide stellar companion candidate. [(d)] Skrutskie et al. (2006); Cutri et al. (2003). [(e)] Expected number of background stars in the NACO S13 field of view (see text).

References. (1) Köhler (2001). (2) Covino et al. (1997). (3) Sartori et al. (2003). (4) Torres (1986). (5) Torres et al. (2006). (6) van Leeuwen (2007). (7) Frink et al. (1998). (8) Ghez et al. (1997). (9) Reipurth et al. (2002). (10) Kraus & Hillenbrand (2007). (11) Simultaneously imaged. by Lafrenière et al. (2008) and by us (here). (12) Luhman (2007). (13) supposed by Neuhäuser et al. (2002). (14) confirmed by Ahmic et al. (2007), Lafrenière et al. (2008) and Schmidt et al. (2008b). (15) Schmidt et al. (2008b). (16) wide companion candidate: Reipurth & Zinnecker (1993), close binary: Brandner (1992), close triple: Brandeker et al. (2001). (17) Possibly SB in Melo (2003) and Torres et al. (2006), but could be the signal of the close triple. (18) Brandner & Zinnecker (1997), Sz 23 (VW Cha D?): Comerón et al. (1999). (19) Damjanov et al. (2007). (20) Lafrenière et al. (2008). (21) Rydgren (1980). (22) SB?: Torres et al. (2006), w*: Kraus & Hillenbrand (2007). (23) **, w*: Brandner (1992); Reipurth & Zinnecker (1993), SB? (primary and secondary in spectrograph entrance window): Reipurth et al. (2002). (24) Hyland et al. (1982). (25) Preibisch (1997).

purpose of the present paper is to present our results for a total of 16 of the 51 Cha members observed with previously known faint stellar companion candidates, which, in most cases, had been observed during only one epoch and, therefore, lack any confirmation of their binary nature. Here we present NACO imaging from one to five different epochs of these objects. Combining our astrometric data with all available literature values, we are able to show that all cases are co-moving binaries or multiple systems, and in many of them there are already indications of orbital motion, partly even curved orbital motion.

In Sect. 2, we describe the details of our observing and reduction strategy. Section 3 summarizes our most important results. Section 4 contains a detailed discussion of each star and Sect. 5 describes the resulting conclusions.

2. Observations and calibrations

All targeted stars with previously known companion candidates, but not yet examined to determine their possible common proper motion, are listed with additional information on the systems in Table 1. These binaries could be recovered within the campaign owing to their proximity to the primaries, fitting within the NACO S13 field of view (1024×1024 pixels = 13.56×13.56 arcsec) during the search for additional fainter companions. In addition to their positions, we list the currently adopted system architecture and the so far known individual spectral types and distances. Finally the 2MASS (Skrutskie et al. 2006; Cutri et al. 2003) brightnesses are given and the last column of Table 1 refers to the expected number of fore- and background stars in each NACO field (1024×1024 pixels = 13.56×13.56 arcsec), according to star counts down to the 2MASS limiting magnitude (near $K = 16$ mag) in a cone of a radius of 300 arcsec around each of the targets. The mean value is 0.117 stars per NACO field, but the individual values vary by a factor ~3. An overview of the current orientation and view of the systems is given in Fig. 1.

In Table 2 we present observational details such as integration times (DIT), the number of combined integrations (NDIT), that is sometimes equivalent to the number of integrations within one cube (which is NDIT in the case of the cube mode), the number of individual integrations or cubes (NINT), and filter bands. In all cases, we used the S13 camera (~13 mas/pixel pixel scale) and the double-correlated read-out mode.

For the raw data reduction, we subtracted a mean dark from all science frames and the flatfield frames, then divided by the normalized dark-subtracted flatfield, and subtracted the mean background using ESO *eclipse/jitter* (Devillard 1997).

We calibrated the NACO data using the wide binary stars HIP 73357 and/or HIP 6445 for our six epochs in 2006–2011. The astrometry of these binaries were measured very accurately by the HIPPARCOS satellite mission (Perryman et al. 1997). However, since these measurements were performed twenty years ago, the binary has possibly undergone a large orbital motion, which now dominates the astrometric uncertainty (see Neuhäuser et al. 2008, for details), resulting in the absolute calibration given in Table 3. Our derived pixel scale is in good agreement with earlier measurements such as e.g. in Neuhäuser et al. (2005, 2008) or Chauvin et al. (2010). The error bars in the pixel scale and orientation increase with time because of the increasing uncertainties in the possible orbital motion of the

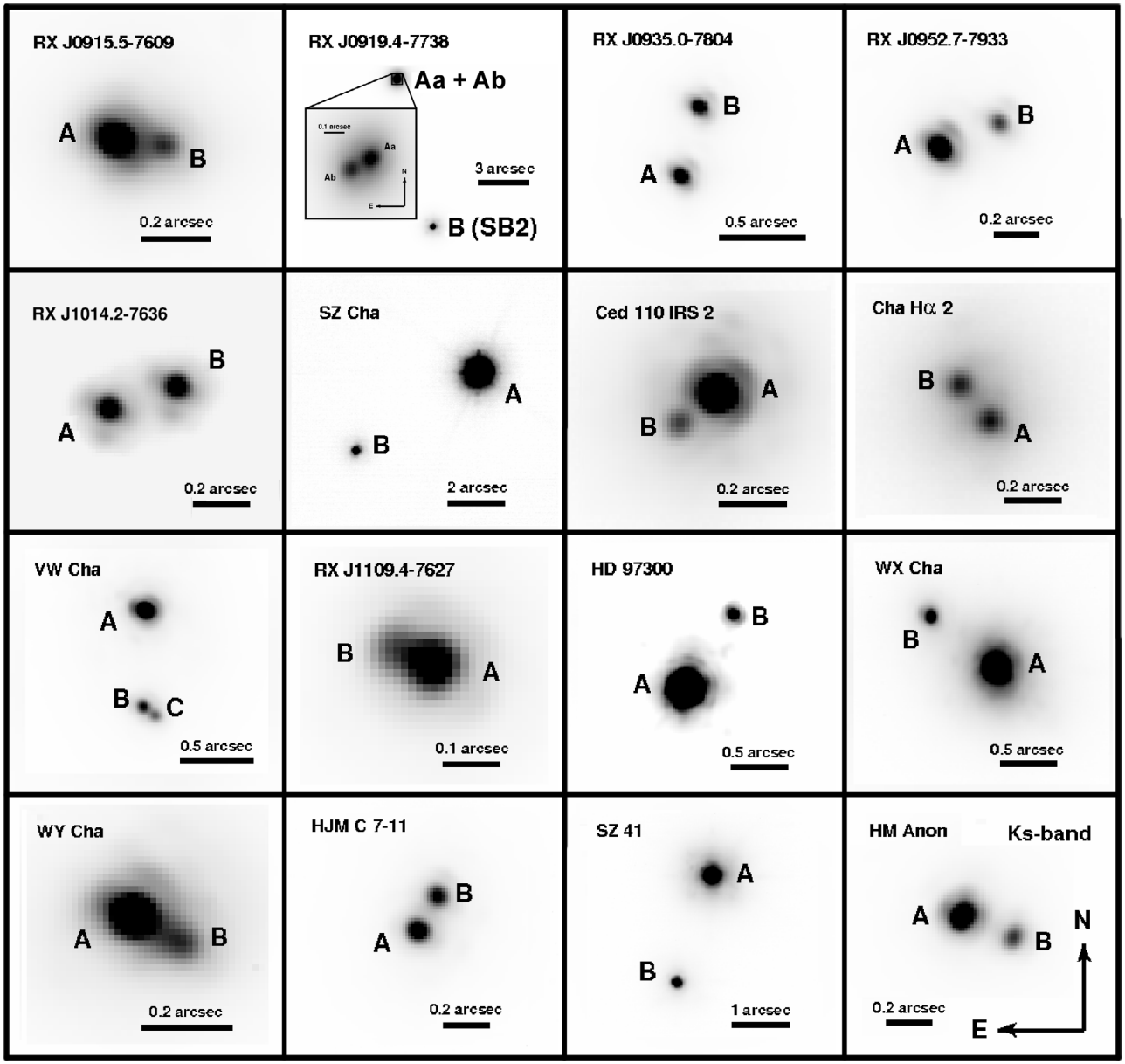

Fig. 1. VLT NACO *Ks* band images of the binary and multiple systems. Spectroscopic binaries are only given if the binarity and component of variation has been reliably determined. Wide stellar companion candidates, marked as w* in Table 1, are outside the FoV of our S13 observations.

calibration binaries. This systematic also dominates the error estimation in terms of the pixel scale and orientation as can easily be seen by the much smaller scatter among the mean values of the pixel scale, independently determined for each epoch, than the individual uncertainties. The given orientation is relative to north in the sky and has to be added to calibrate any measurement done in the images.

Since in Table 3 a trend of increasing orientation by about 0.16°/yr might be present, we checked whether this tentative trend could be due to the orbital motion of the adopted calibration binary HIP 73357. To achieve this, we requested all obervational data of the binary from the Washington Double Star Catalog (WDS) (Mason et al. 2001) from 1835 until 1998 in the version of April 4 2007 and found the binary to have an orbital motion from –0.01 to –0.04°/yr in position angle, neglecting two outliers, and less than –0.01°/yr within the past 50 years. Owing to the lack of error bars in the data, we cannot give precise numbers, although since the orbital motion seems to be negligible we calibrated each measurement by the orientation value given in Table 3, taking the maximal possible orbital motion of a circular orbit according to Kepler's third law into account in the error budget.

3. Astrometric and photometric results

3.1. Astrometry

To verify the common proper motion of the tentative companions of our targets (Table 1), we used the proper motion (PM) of the stars published in the literature (Table 4) to calculate the expected change in the separation and position angle of the respective components based on the hypothesis that one of the components is a non-moving background star. We used either the newest values combining most of the previous data with new measurements, in this case of UCAC3 (Zacharias et al. 2010) combining data from about 140 catalogues, or the weighted

Table 2. VLT/NACO observation log.

Object	Other name	JD – 2 453 700 [days]	Date of observation	DIT [s]	NDIT	Number of images	Airmass	Seeing [arcsec]	Filter
RX J0915.5-7609	RX J0915.5-7608	461.53412	2 Mar. 2007	2.2	28	20	1.73	1.04	*Ks*
		1181.59508[a]	19 Feb. 2009	2	30	6	1.66	0.88	*Ks*
RX J0919.4-7738	HIP 45734	815.51911	19 Feb. 2008	1.2	50	30	1.92	0.99	*Ks*
RX J0935.0-7804	2MASS J09345604	461.59183	2 Mar. 2007	7	9	30	1.71	1.22	*Ks*
	-7804193	814.61953	18 Feb. 2008	11	6	28	1.72	1.13	*Ks*
		815.58352	19 Feb. 2008	30	2	38	1.78	1.05	*J*
		1182.58189[a]	20 Feb. 2009	3	20	30	1.77	0.73	*Ks*
RX J0952.7-7933	HD 86588	460.58336	1 Mar. 2007	2.5/1.5	25/40	10/12	1.81	1.26	*Ks*
		814.64850	18 Feb. 2008	3	20	13	1.76	1.01	*Ks*
		814.65931	18 Feb. 2008	3	20	6	1.75	0.90	*J*
		1181.63897[a]	19 Feb. 2009	1	60	10	1.77	0.68	*Ks*
		1181.64617[a]	19 Feb. 2009	0.5	120	5	1.76	0.69	*H*
		1181.65104[a]	19 Feb. 2009	1.5	40	5	1.76	0.72	*J*
		1550.53614[a]	23 Feb. 2010	0.347	126	10	1.96	0.86	*Ks*
		1853.86365[a]	23 Dec 2010	3	20	30	1.74	2.21	*Ks*
		1945.57285[a]	25 Mar. 2011	0.347	126	10	1.75	1.11	*Ks*
RX J1014.2-7636	2MASS J10140807	1550.56298[a]	23 Feb. 2010	0.347	126	42	1.83	0.88	*Ks*
	-7636327	1945.60036[a]	25 Mar. 2011	0.347	126	42	1.63	1.11	*Ks*
SZ Cha	Ass Cha T 2-6	82.64912	16 Feb. 2006	1	50	20	1.75	0.73	*Ks*
		1181.66756[a]	19 Feb. 2009	0.5	120	22	1.70	0.65	*Ks*
Ced 110 IRS 2	Ass Cha T 2-21	82.61949	16 Feb. 2006	0.3454	100	20	1.85	0.75	*Ks*
		815.61187	19 Feb. 2008	0.3454	174	5	1.85	0.78	*Ks*
		815.61683	19 Feb. 2008	0.5	120	5	1.84	0.80	*J*
Cha Hα 2	ISO-ChaI 111	82.68981	16 Feb. 2006	10	6	20	1.70	0.63	*Ks*
		460.71934	1 Mar. 2007	60	2	15	1.66	1.15	*Ks*
		461.67171	2 Mar. 2007	30	2	24	1.68	1.20	*J*
VW Cha	Ass Cha T 2-31	83.90711	17 Feb. 2006	0.3454	100	20	1.94	0.49	*Ks*
RX J1109.4-7627	CHXR 37	1182.81186[a]	20 Feb. 2009	2	30	6	1.67	0.57	*Ks*
		1551.69870[a]	24 Feb. 2010	0.347	126	12	1.63	1.00	*Ks*
HD 97300	Ass Cha T 2-41	460.60766	1 Mar. 2007	0.5	110	20	1.77	1.23	*Ks*
		816.71442	20 Feb. 2008	0.5	120	5	1.63	0.80	*Ks*
		816.71936	20 Feb. 2008	0.3454	174	5	1.63	0.87	*J*
WX Cha	Ass Cha T 2-45	1181.91858[a]	19 Feb. 2009	2	30	6	2.00	0.76	*Ks*
WY Cha	Ass Cha T 2-46	816.70106	20 Feb. 2008	2	30	5	1.64	0.68	*Ks*
		816.70577	20 Feb. 2008	7.5	8	5	1.64	0.73	*J*
HJM C 7-11	CHXR 47	461.78979	2 Mar. 2007	2	30	21	1.71	1.41	*Ks*
		815.79485	19 Feb. 2008	2	30	21	1.68	0.53	*Ks*
		1181.70578[a]	19 Feb. 2009	1.5	40	36	1.67	0.52	*Ks*
		1181.77101[a]	19 Feb. 2009	1.5	40	17	1.66	0.50	*H*
		1181.78711[a]	19 Feb. 2009	10	6	15	1.67	0.67	*J*
Sz 41	Ass Cha T 2-51	1181.88546[a]	19 Feb. 2009	1.5	40	6	1.84	0.81	*Ks*
		1550.08623[a]	23 Feb. 2010	0.347	126	42	1.83	1.16	*Ks*
HM Anon	Ass Cha T 2-54	815.69528	19 Feb. 2008	1	60	12	1.68	0.57	*Ks*
		815.70581	19 Feb. 2008	2	30	12	1.67	0.56	*J*
		1182.87337[a]	20 Feb. 2009	1	60	32	1.84	0.52	*Ks*

Notes. Each image consists of the number of exposures given in Col. 6 multiplied by the individual integration time given in Col. 5. [(a)] Data taken in cube mode, hence each image is a cube of the number of planes given in Col. 6, each having the individual integration time given in Col. 5.

mean proper motion of several independent measurements, as for Cha Hα 2 (see e.g. Schmidt et al. 2008b), which was previously supposed to be a faint brown dwarf candidate and whose data were in part derived by us from SuperCOSMOS Sky Survey (SSS) data (Hambly et al. 2001) and NTT/SofI and VLT/FORS measurements (see Table 4), to check whether the objects have a common PM, as we describe in the following sections. For comparison, we give in addition the median proper motion value of the Chamaeleon I association derived from the UCAC2 (Zacharias et al. 2004) data by Luhman et al. (2008) in Table 4.

To determine the positions of both components, we constructed a reference point spread function (PSF) from both objects. Thus, we obtained an appropriate reference PSF for each single image. Using IDL/starfinder (Diolaiti et al. 2000), we scaled and shifted the reference PSF simultaneously to both components in each of our individual images by minimizing the residuals. Realistic error estimates in both the position and flux of each object were obtained from the mean and standard deviation in the positions found in all individual images of a single epoch. When the objects are either too close or their brightness difference is too strong, we subtracted the PSF of each component using an IDL rotation routine (described in more detail in Neuhäuser et al. 2008) before measuring the astrometry and photometry of the other component, respectively.

As already discussed in the previous section, we used the HIPPARCOS binary HIP 73357 to calibrate our images. Hence,

Table 3. Astrometric calibration results using the binary HIP 73357.

JD – 2 453 700 [days]	Epoch	Pixel scale [mas/pixel]	Orientation [°]	Filter
88.84779	Feb. 2006	13.24 ± 0.18	0.18 ± 1.24	*Ks*
460.84330	Mar. 2007	13.24 ± 0.19	0.33 ± 1.32	*Ks*
815.91117	Feb. 2008	13.22 ± 0.20	0.73 ± 1.40	*J*
815.91907	Feb. 2008	13.25 ± 0.20	0.68 ± 1.40	*Ks*
1181.89936	Feb. 2009	13.25 ± 0.21	0.76 ± 1.48	*Ks*
1550.82276	Feb. 2010	13.24 ± 0.22	0.72 ± 1.56	*Ks*
1854.54334	Dec. 2010[a]	13.23 ± 0.23	0.95 ± 1.63	*Ks*
1945.86023	Mar. 2011	13.24 ± 0.24	1.00 ± 1.65	*Ks*

Notes. The values of HIPPARCOS (Perryman et al. 1997) were used as reference values. Measurement errors of HIPPARCOS as well as maximum possible orbital motion since the epoch of the HIPPARCOS observation are taken into account. [(a)] Although HIP 73357 was not observed in Dec. 2010, HIP 6445, observed in Feb. 2010 and Dec. 2010, could be used to transfer the HIP 73357 calibration to Dec. 2010.

the uncertainties in the absolute astrometric results, given in Table 9, include the uncertainties in the HIPPARCOS astrometry, the maximum possible orbital motion of the calibration binary and the measurement errors in the position of the targets and their companions. In Table 9, we list the separation between the components (ρ) with its uncertainty (δ_ρ), the position angle (PA) with its uncertainty ($\delta_{\rm PA}$), as well as the significance of a measurement at epoch i not being a background object ($\sigma_{\rho,\,{\rm back},\,i}$ and $\sigma_{{\rm PA},\,{\rm back},\,i}$). We calculated $\sigma_{\rho,\,{\rm back},\,i}$ and $\sigma_{{\rm PA},\,{\rm back},\,i}$ from the measured difference in the separation and position angle of the components between epoch i and the corresponding expected values at the Julian date of epoch i in the case of the fainter component being a non-moving background object by extrapolating the known proper motions of the primaries (Table 4) with respect to the (latest) reference epoch with index 0, via

$$\sigma_{\rho,\,{\rm back},\,i} = \frac{\rho_i - \rho_{{\rm back}_i}(\rho_0)}{\sqrt{\delta^2_{\rho_i} + \delta^2_{\rho_{{\rm back}_i}}(\delta_{\rho_0})}}, \quad (1)$$

$$\sigma_{{\rm PA},\,{\rm back},\,i} = \frac{{\rm PA}_i - {\rm PA}_{{\rm back}_i}({\rm PA}_0)}{\sqrt{\delta^2_{{\rm PA}_i} + \delta^2_{{\rm PA}_{{\rm back}_i}}(\delta_{{\rm PA}_0})}}, \quad (2)$$

where for instance $\rho_{{\rm back}_i}(\rho_0)$ would be the expected separation of the components if the fainter of the two were a background object. The parameter $\delta_{{\rm back}_i}(\delta_0)$ is the associated uncertainty in that value, which is essentially the width of the background cone at epoch i relative to the (latest) reference measurement 0 taking into account the proper motion uncertainty, the measurement uncertainty at the reference epoch, and the brightness difference between the components. The last quantity influences the measured proper motion of the combined light.

Finally, the likelihood that a measurement i represents orbital motion is calculated similarly for each epoch as a measure of the deviations in the separation and position angle from the reference epoch with index 0, via

$$\sigma_{\rho,\,{\rm orb},\,i} = \frac{\rho_i - \rho_0}{\sqrt{\delta^2_{\rho_i} + \delta^2_{\rho_0}}}, \quad (3)$$

$$\sigma_{{\rm PA},\,{\rm orb},\,i} = \frac{{\rm PA}_i - {\rm PA}_0}{\sqrt{\delta^2_{{\rm PA}_i} + \delta^2_{{\rm PA}_0}}}. \quad (4)$$

All values are given in Table 9.

Table 4. Proper motions.

Object	Reference	$\mu_\alpha \cos\delta$ [mas/yr]	μ_δ [mas/yr]
RX J0915.5 –7609	UCAC 3 (1)	–29.3 ± 2.0	18.9 ± 1.4
RX J0919.4 –7738	HIPPARCOS (new) (2)	–109.7 ± 0.88	72.35 ± 0.8
	Tycho-2 (3)	–82.0 ± 11.3	73.10 ± 7.7
	PPMX (4)	–108.19 ± 1.5	68.28 ± 1.6
	used: UCAC 3 (1)	–105.3 ± 1.2	72.1 ± 1.2
RX J0935.0 –7804	UCAC 3 (1)	–28.6 ± 1.3	19.2 ± 1.3
RX J0952.7 –7933	UCAC 3 (1)	–13.5 ± 0.9	2.0 ± 0.9
RX J1014.2 –7636	UCAC 3 (1)	–47.2 ± 1.7	30.6 ± 3.6
SZ Cha	UCAC 3 (1)	–22.5 ± 6.9	1.7 ± 2.7
Ced 110 IRS 2	UCAC 3 (1)	–19.2 ± 1.0	5.0 ± 1.6
Cha Hα 2	PSSPMC (5)	–23 ± 17	1 ± 17
	SSS-FORS1 (6)	–19.4 ± 14.9	–0.3 ± 14.9
	SSS-SofI (6)	–23.0 ± 14.1	7.8 ± 14.1
	weighted mean	–21.75 ± 8.77	3.18 ± 8.77
VW Cha	UCAC 3 (1)	–19.7 ± 1.3	–0.8 ± 3.4
RX J1109.4 –7627	UCAC 3 (1)	–22.3 ± 1.8	–0.8 ± 9.9
HD 97300	HIPPARCOS (new) (2)	–21.63 ± 0.94	–0.72 ± 0.78
	Tycho-2 (3)	–19.1 ± 1.4	–0.1 ± 1.4
	PPMX (4)	–21.01 ± 1.4	–0.48 ± 1.5
	used: UCAC 3 (1)	–17.7 ± 1.0	–2.7 ± 1.1
WX Cha	UCAC 3 (1)	–20.9 ± 1.7	–0.6 ± 2.3
WY Cha	ICRF extension (7)	–7 ± 13	11 ± 11
	used: UCAC 3 (1)	–22.2 ± 1.8	–0.5 ± 1.8
HJM C7-11	UCAC 3 (1)	–20.3 ± 1.8	1.7 ± 1.8
Sz 41	ICRF extension (7)	–15 ± 5	9 ± 4
	used: UCAC 3 (1)	–29.8 ± 4.3	4.7 ± 1.7
HM Anon	Tycho-2[a] (3)	–17.5 ± 5.7	–72.3 ± 5.5
	used: UCAC 3 (1)	–21.6 ± 1.0	4.8 ± 1.0
Median Cha I	Luhman[b] (8)	–21 ± ∼1	2 ± ∼1

Notes. Only independent sources with individual error bars for the targets were taken into account. [(a)] As given in Skiff (2009), the Tycho-2 coordinates are wrong and HM Anon equals TYC 9414-1250-1. [(b)] Based on UCAC2 proper motions from (9).
References. (1) Zacharias et al. (2010). (2) van Leeuwen (2007). (3) Høg et al. (2000). (4) Röser et al. (2008). (5) Ducourant et al. (2005). (6) Schmidt et al. (2008b); Hambly et al. (2001). (7) Camargo et al. (2003). (8) Luhman et al. (2008). (9) Zacharias et al. (2004).

In addition, we performed relative astrometric measurements between the components for our common proper motion analysis, which allows a more precise determination of the common

Table 5. Relative astrometric results.

Object	Epoch difference [days] Δt	Change in separation [pixel] $\Delta\rho \pm \delta_{\Delta\rho}$	Sign.[a,c] not Backg. $\sigma_{\rho,\mathrm{back}}$	Sign.[c] orb. motion $\sigma_{\rho,\mathrm{orb}}$	Change in PA[b] [°] $\Delta\,\mathrm{PA} \pm \delta_{\Delta\,\mathrm{PA}}$	Sign.[a,c] not Backg. $\sigma_{\mathrm{PA,back}}$	Sign.[c] orb. motion $\sigma_{\mathrm{PA,orb}}$
RX J0915.5-7609 AB	720.06096	–0.784 ± 0.417	7.9	1.9	–3.476 ± 1.330	9.3	2.6
RX J0935.0-7804 AB	720.99006	0.564 ± 0.096	21	5.9	–1.210 ± 0.229	17	5.3
	367.48036	0.317 ± 0.077	18	4.1	–0.557 ± 0.156	16	3.6
RXJ0952.7-7933 AB	1484.98949	–0.192 ± 0.128	13	1.5	–7.690 ± 0.460	10	17
	1130.91894	–0.087 ± 0.086	14	1.0	–6.586 ± 0.285	11	23
	763.93388	0.064 ± 0.132	12	0.5	–4.405 ± 0.288	9.4	15
	395.03671	0.161 ± 0.039	15	4.1	–2.199 ± 0.115	7.2	19
	91.70920	0.055 ± 0.039	8.3	1.4	–0.394 ± 0.080	3.4	4.9
RX J1014.2-7636 AB	395.03738	0.889 ± 0.045	27	20	–2.163 ± 0.184	2.3	12
SZ Cha AB	1099.01844	0.289 ± 1.050	2.5	0.3	–0.006 ± 0.250	1.2	0.0
Ced 110 IRS 2 AB	732.99238	–0.404 ± 0.281	9.8	1.4	–6.244 ± 1.466	0.4	4.3
Cha Hα 2 AB	378.02953	–0.573 ± 0.188	1.5	3.1	0.375 ± 0.875	2.1	0.4
RXJ1109.4-7627 AB	1431.18790	–0.526 ± 0.190	0.8	2.8	–23.727 ± 1.292	3.4	18
	368.88684	–0.422 ± 0.195	3.1	2.2	–8.216 ± 1.395	2,1	5.9
HD 97300 AB	695.81337	–0.271 ± 0.123	4.2	2.2	–0.505 ± 0.177	12	2.9
	356.10676	–0.064 ± 0.078	4.0	0.8	–0.419 ± 0.096	12	4.3
WX Cha AB	1062.02756	0.028 ± 0.303	6.8	0.1	0.333 ± 0.375	4.4	0.9
WY Cha AB	697.06258	–0.106 ± 0.214	8.7	0.5	–0.962 ± 0.819	4.2	1.2
HJM C 7-11 AB	1062.12708	–0.208 ± 0.258	7.0	0.8	–2.925 ± 0.784	10	3.7
	719.91599	–0.224 ± 0.275	5.9	0.8	–1.177 ± 1.229	7.9	1.0
	365.91093	–0.033 ± 0.149	5.5	0.2	–0.783 ± 0.676	8.1	1.2
Sz 41 AB	1430.54160	0.359 ± 0.529	4.6	0.7	0.125 ± 0.328	5.7	0.4
	368.20077	0.056 ± 0.154	4.3	0.4	0.177 ± 0.089	6.5	2.0
HM Anon AB	1062.00560	–0.378 ± 0.059	16	6.4	1.248 ± 0.257	13	4.8
	648.39052	–0.271 ± 0.041	15	6.6	0.679 ± 0.174	11	3.9
	367.17809	–0.156 ± 0.035	14	4.5	0.356 ± 0.130	9.0	2.7

Notes. [(a)] Assuming the fainter component is a non-moving background star . [(b)] PA is measured from N over E to S. [(c)] Significances are given relative to the last epoch.

proper motion and orbital motion for measurements taken with the same instrument. Relative astrometric measurements deal only with the changes in the separation and position angles between the observed epochs, hence relaxes the constraints on the astrometric calibration. The calibration takes into account only the uncertainties in separation, position angle, and proper motion of the target, as well as the uncertainties in the separation, position angle, and possible orbital motion of the calibration binary between the NACO epochs (here 2006–2011). The possible maximal orbital motion of the calibration binary was calculated only for 2006–2011 (or less), hence the final errors in the relative astrometric measurements for our targets are smaller and changes in these values can be recovered with higher significance, although no absolute reference for separation and PA can be given. We refer to Neuhäuser et al. (2008) for a further discussion of this concept. This allows precise measurement of the relative motions of the targets and the companion candidates given in Table 5. Analogues to the formulas given in the last paragraph, the significances for not being a background object and for orbital motion from relative astrometric measurements are given in Table 5, calculated using the time difference (Δt) between measurements as well as the change in separation ($\Delta\rho$) and position angle (ΔPA) and their uncertainties. The absolute astrometric measurements between the components (Table 9) must instead incorporate the full uncertainties of the astrometric calibration (given in Table 3). We emphasize that common proper motion can mostly be shown much more precisely based on relative astrometric measurements, while absolute values are given for future comparisons, also with different instruments.

Finally, we performed a linear orbital movement analysis for the absolute and relative astrometric results given in Tables 9 and 5 in order to check whether the first indications of orbital motion of the systems can already be found after a few years of observations, since the orbital periods of the projected orbital separations (for circular orbits) is beyond 15 years in all cases, mostly beyond or significantly beyond 50 years. In Tables 6 and 7 we provide the results of these analysis as well as the projected spatial separations, according to the minimal observed separation in Table 9 and the adopted distance given in Table 1. In addition, the only comparison value found by us in the literature for the star HM Anon is listed there, after conversion of the values from km/s to mas/yr using the distance to Cha I of 160 pc as assumed in the source paper of Woitas et al. (2001) and originally given in Wichmann et al. (1998).

3.2. Photometry

As described in Sect. 3.1, from the PSF fitting of both components we also obtained their flux ratio, which is given for each pair in Table 8. Owing to the lack of photometric conditions or photometric calibrators in different nights, we are unable to provide the individual brightnesses of the objects. However, we calculated the mean brightness of each individual object by assuming the combined brightness of the objects, measured by 2MASS (Skrutskie et al. 2006) in one epoch, and dividing the brightness according to our measured flux ratios in each band. However, we should remember that all of the objects are young and thus likely variable, so that we give these values in Table 8 with reservations

as a preliminary orientation for the reader only and hence, without error bars.

4. Description of the individual targets

4.1. The proper motion diagram (PMD)

To analyse and interpret the astrometric data we apply a "proper motion diagram" (PMD), which contains the measured values of either the separation or the position angle with their errors versus time (Fig. 2). In each case, we consider the hypothesis that the fainter component of the supposed binary is a non-moving background star. The proper motions in Table 4 are obtained by evaluating the centroid measurements of the unresolved system, or they are proper motions of unresolved systems from literature catalogs, except for the resolved system RX J0919.4-7738, which was treated accordingly. Hence, if the fainter component is a non-moving background object, the true proper motion of the brighter object must be corrected to ensure that the centroid reproduces the observed proper motion. For this purpose, the formulas given by the Astronomical Almanac 2005 of the US Government Printing Office (Usgpo) (2003) were applied. The location and movement of the centroid was determined according to the apparent Ks magnitudes in Table 8. The corrected proper motion values of the brighter components were used to calculate the separations and position angles, which gives the dashed-dotted central line in the PMD, surrounded by solid lines according to the errors in the proper motions. The waves in these curves are due to the differential parallactic motion of the brighter component, which depends on the adopted distance; for the non-moving background object, we assume a parallax of zero. In most cases, we used the mean value 165 pc for Cha I (based on the data of Bertout et al. 1999; and Whittet et al. 1997; see Schmidt et al. 2008a, for more information); different distance values are mentioned in the description of individual stars in Table 1.

The long-dashed lines in the PMD enclose the area of constant separation (or position angle), while the opening short-dashed cone indicates the range of maximal amplitudes of the circular orbital motions according to Kepler's third law. Here we used our photometry in Table 8 and converted the Ks magnitudes into mass estimates according to the models of Baraffe et al. (1998). Assumed edge-on orbits define the maximal variations in the separation, while face-on orbits cause maximal variations in the position angle.

The PMDs confirm that all 16 binaries and multiple systems are co-moving, which can also be concluded from the significances $\sigma_{\rho,\,\mathrm{back}}$ and $\sigma_{\mathrm{PA},\,\mathrm{back}}$ that the faint object is not a background star. The relative astrometric measurements (Table 5) give for both of them combined always $\sigma > 2.8$. The slopes of the linear least square fits through the individual data points in the PMDs and their errors are listed in Table 6 for the absolute astrometric measurements and in Table 7 for the relative astrometric measurements.

In principle, the a priori hypothesis that the fainter component is a background star is arbitrary. It could be that the brighter component is a projected distant, but more luminous non-member while the fainter one belongs to the Cha complex. The corresponding calculations were carried out and revealed that the resulting changes in the significances for not being a background object are insignificant in the case of co-moving systems, as for all objects in this paper. Hence, these reversed PMDs are therefore not considered in greater detail.

Table 6. Projected orbital separations and linear orbital movement fit results from absolute astrometric measurements.

Object	Proj. sep. [AU]	Change in separation [mas/yr]	Change in PA[a] [°/yr]
RX J0915.5-7609 AB	25	2.77[b] ± 0.64	–2.58 ± 0.37
RX J0919.4-7738			
(AaAb)B[c]	511	–2.97 ± 5.64	0.07 ± 0.06
AaAb	6	–0.17 ± 0.39	–4.10 ± 0.20
RX J0935.0-7804 AB	69	4.61 ± 0.37	–0.65 ± 0.06
RX J0952.7-7933 AB	47	1.14[b] ± 0.26	–1.65[b] ± 0.06
RX J1014.2-7636 AB	41	10.67 ± 0.53	1.94[b] ± 0.45
SZ Cha AB	845	0.26 ± 2.44	0.01 ± 0.07
Ced 110 IRS 2 AB	24	–2.18 ± 2.32	–2.95 ± 1.15
Cha Hα 2 AB	35	–4.09 ± 2.20	0.57 ± 0.83
VW Cha A(BC)[d]	120	–0.98 ± 0.57	0.27 ± 0.07
BC	19	–3.59[b] ± 0.42	–0.57 ± 0.26
RX J1109.4-7627 AB	13	–1.34 ± 0.69	–5.82 ± 0.55
HD 97300 AB	139	–4.10 ± 2.96	–0.02 ± 0.16
WX Cha AB	130	–2.48 ± 2.70	–0.19 ± 0.16
WY Cha AB	20	–0.73 ± 2.00	–0.50 ± 1.07
HJM C7-11 AB	29	–1.11[e] ± 1.63	–0.39 ± 0.33
Sz 41 AB	326	–0.97 ± 2.28	–0.03 ± 0.10
HM Anon AB	45	–1.77 ± 1.35	0.75 ± 0.33

Notes. [(a)] PA is measured from N over E to S. [(b)] Possible indications present for curved orbital motion. [(c)] See [d] in Table 9. [(d)] See [e] in Table 8. [(e)] Not using the data point by Ghez et al. (1997) given in Table 9.

Table 7. Projected orbital separations and linear orbital movement fit results from relative astrometric measurements.

Object	Proj. sep. [AU]	Change in separation [mas/yr][a]	Change in PA[b] [°/yr]
RX J0915.5-7609 AB	25	–5.26 ± 2.80	–1.76 ± 0.67
RX J0935.0-7804 AB	69	3.88 ± 0.59	–0.59 ± 0.10
RX J0952.7-7933 AB	47	0.02[c] ± 0.25	–2.04[c] ± 0.06
RX J1014.2-7636 AB	41	10.88 ± 0.56	–2.00 ± 0.17
SZ Cha AB	845	1.27 ± 4.62	0.00 ± 0.08
Ced 110 IRS 2 AB	24	–2.66 ± 1.85	–3.11 ± 0.73
Cha Hα 2 AB	35	–7.35 ± 2.40	0.36 ± 0.85
RX J1109.4-7627 AB	13	–1.31 ± 0.58	–5.76 ± 0.28
HD 97300 AB	139	–1.52 ± 0.75	–0.34 ± 0.07
WX Cha AB	130	0.13 ± 1.38	0.11 ± 0.13
WY Cha AB	20	–0.73 ± 1.48	–0.50 ± 0.43
HJM C7-11 AB	29	–0.98 ± 0.94	–0.93 ± 0.24
Sz 41 AB	326	1.00 ± 1.36	0.10 ± 0.06
HM Anon AB	45	–1.86 ± 0.21	0.40 ± 0.07

Notes. [(a)] Using a nominal pixel scale of 0.01324 arcsec/pixel to convert from pixel to mas. [(b)] PA is measured from N over E to S. [(c)] Possible indications present for curved orbital motion.

Moving background stars can only be rejected if curved orbital motion is detected.

In only a few remarkable cases are the corresponding PMDs shown in the following sections. A typical example is given in Fig. 2. The remaining PMDs are in the online appendix.

4.2. Co-moving binaries without orbit indications

We discuss here three stars that are co-moving but for which we could not detect orbital motions. Their significance in relative

Table 8. Measured brightness differences and mean apparent magnitudes.

Object	Epoch	J-band [mag]	H-band [mag]	Ks-band [mag]	Object	J-band [mag]	H-band [mag]	Ks-band [mag]
RX J0915.5-7609 A-B	2 Mar. 2007			1.501 ± 0.023	A			8.736
	19 Feb. 2009			1.448 ± 0.081	B			10.212
RX J0919.4-7738 Aa-B	19 Feb. 2008			0.796 ± 0.130	Aa			8.236
Ab-B				1.141 ± 0.114	Ab			8.581
Aa-Ab				0.344 ± 0.043	B*[d]			7.440
RX J0935.0-7804 A-B	2 Mar. 2007			0.113 ± 0.021	A	10.482		9.587
	18/19 Feb. 2008	0.133 ± 0.009		0.100 ± 0.118	B	10.615		9.701
	20 Feb. 2009			0.130 ± 0.015				
RX J0952.7-7933 A-B	1 Mar. 2007			1.575 ± 0.055	A	8.580	8.307	8.244
	18 Feb. 2008	1.541 ± 0.017		1.647 ± 0.148	B	10.127	9.944	9.718
	19 Feb. 2009	1.553 ± 0.020	1.637 ± 0.256	1.486 ± 0.059				
	23 Feb. 2010			1.411 ± 0.014				
	23 Dec. 2010			1.365 ± 0.017				
	25 Mar. 2011			1.361 ± 0.014				
RX J1014.2-7636 A-B	23 Feb. 2010			0.073 ± 0.014	A			9.598
	25 Mar. 2011			0.045 ± 0.010	B			9.656
SZ Cha A-B	16 Feb. 2006			3.518 ± 0.050	A*			7.758
	19 Feb. 2009			3.406 ± 0.031	B			11.220
Ced 110 IRS 2 A-B	16 Feb. 2006			2.358 ± 0.060	A	7.689		6.529
	19 Feb. 2008	2.628 ± 0.011		2.507 ± 0.007	B	10.318		8.962
Cha Hα 2 A-B	25 Mar. 2005[a,b]			0.085 ± 0.028	A	12.906		11.374
	16 Feb. 2006			0.111 ± 0.032	B	13.023		11.484
	1/2 Mar. 2007	0.116 ± 0.048		0.135 ± 0.065				
VW Cha A-B	17 Feb. 2006			1.663 ± 0.007	A			7.280
A-C				2.268 ± 0.006	B			8.943
B-C				0.605 ± 0.005	C			9.548
RX J1109.4-7627 A-B	26 Mar. 2006[c]		1.174 ± 0.008	1.089 ± 0.010	A		9.361	9.033
	20 Feb. 2009			1.175 ± 0.005	B		10.535	10.149
	24 Feb. 2010			1.084 ± 0.020				
HD 97300 A-B	26 Mar. 2006[c]		3.463 ± 0.054	3.119 ± 0.017	A	7.673	7.391	7.215
	1 Mar. 2007			2.946 ± 0.010	B	11.478	10.854	10.224
	20 Feb. 2008	3.805 ± 0.016		2.962 ± 0.023				
WX Cha A-B	25 Mar. 2006[c]		2.276 ± 0.034	2.678 ± 0.023	A		8.894	8.073
	19 Feb. 2009			2.356 ± 0.020	B		11.170	10.590
WY Cha A-B	25 Mar. 2006[c]		1.554 ± 0.058	1.773 ± 0.018	A	10.205	9.197	8.678
	20 Feb. 2008	1.268 ± 0.004		1.415 ± 0.004	B	11.473	10.751	10.272
HJM C7-11 A-B	25 Mar. 2006[c]		0.490 ± 0.018	0.520 ± 0.029	A	10.280	9.241	8.813
	2 Mar. 2007			0.596 ± 0.058	B	10.759	9.684	9.303
	19 Feb. 2008			0.472 ± 0.027				
	19 Feb. 2009	0.479 ± 0.004	0.397 ± 0.024	0.373 ± 0.018				
Sz 41 A-B	25 Mar. 2006[c]		2.571 ± 0.116	2.351 ± 0.039	A		8.622	8.137
	19 Feb. 2009			1.999 ± 0.008	B		11.193	10.315
	23 Feb. 2010			2.185 ± 0.028				
HM Anon A-B	26 Mar. 2006[c]			1.486 ± 0.012	A	8.853	8.285	8.137
	13 May 2007[c]	1.763 ± 0.023	1.500 ± 0.009	1.443 ± 0.013	B	10.542	9.786	9.572
	19 Feb. 2008	1.615 ± 0.019		1.386 ± 0.006				
	20 Feb. 2009			1.426 ± 0.017				

Notes. Mean apparent magnitudes based on combined brightness measurements of 2MASS (Skrutskie et al. 2006). In case of resolved measurements by 2MASS the component for which the brightness was used is marked by a *. [(a)] Schmidt et al. (2008b), improved. [(b)] See also Ahmic et al. (2007) and Lafrenière et al. (2008). [(c)] Rereduced, see also Lafrenière et al. (2008). [(d)] Aa+Ab are slightly brighter than B, being itself an unresolved spectroscopic binary (SB2).

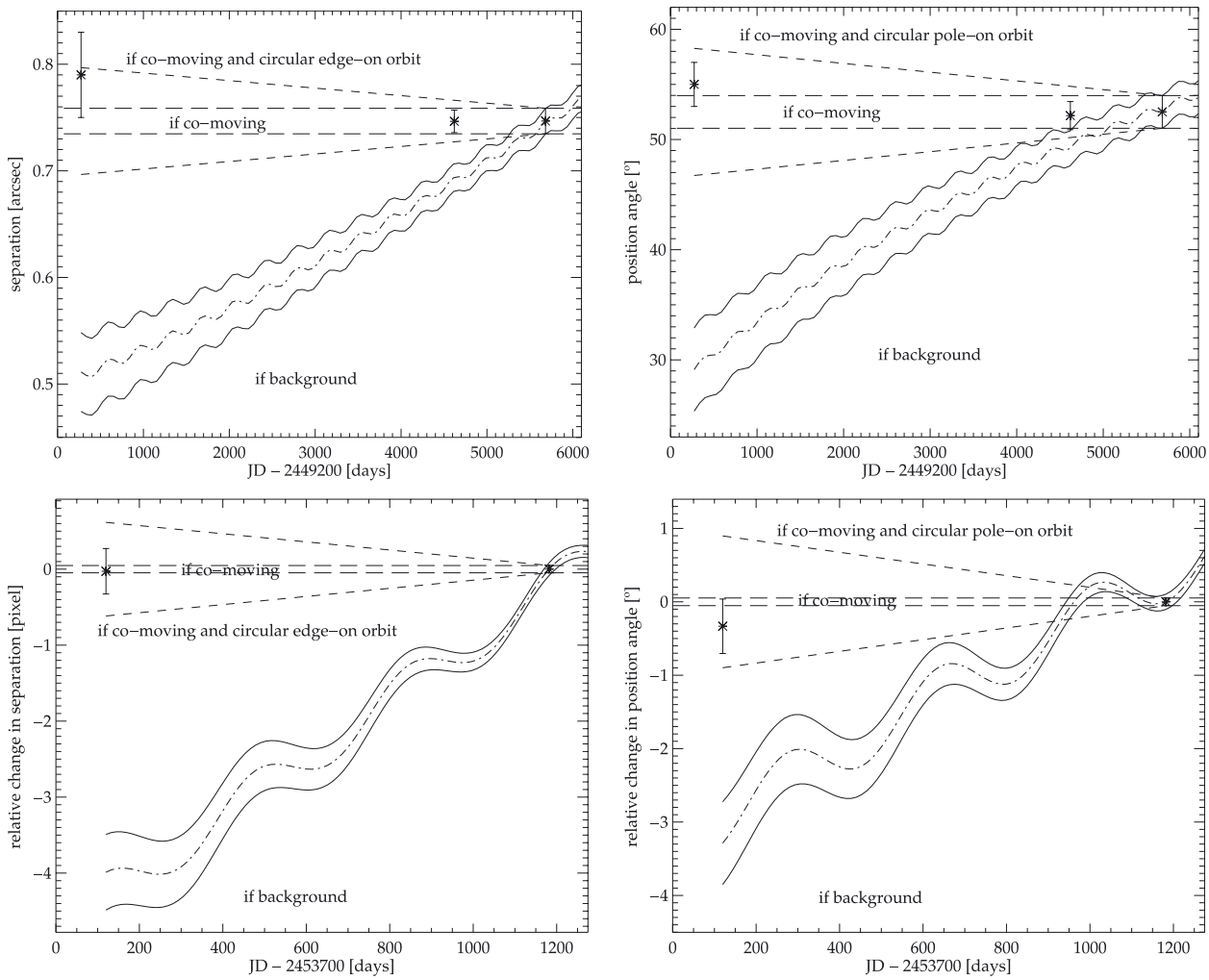

Fig. 2. Example proper motion diagrams (PMD) for separation and position angle change (*left to right*) from both absolute astrometric measurements (*top*) and from relative astrometric measurements (*bottom*) in the WX Cha AB system. The long dashed lines enclose the area for constant separation, as expected for a co-moving object. The dash-dotted line is the change expected if the WX Cha companion is a non-moving background star. The opening cone enclosed by the continuous lines its estimated errors. The waves of this cone show the differential parallactic motion that has to be taken into account if the other component is a non-moving background star with negligible parallax. The opening short-dashed cone represents a combination of co-motion and the maximum possible orbital motion for a circular edge-on orbit (for separation) or circular pole-on orbit (for PA). See text for more information.

astrometric measurements is $\sigma_{\rm orb} \leq 1.2\ \sigma$ (see Table 5). Consequently, their slopes in separation and position angles are also insignificant (see Tables 6 and 7).

SZ Cha

With about a 5 arcsec separation, this is the widest here reported binary. The first measurement by Ghez et al. (1997) has a rather large error. The absolute PMD (Fig. A.6) is therefore compatible with a co-moving binary, but we can exclude from these values the background hypothesis of a non-moving fainter star in the background by 2.8σ. However, in the relative PMDs we can exclude this possibility with a 3.0σ significance based on a time difference Δt of only 3 years instead of almost 15 years in the absolute comparison. In Table 9, we did not include a measurement by Ageorges et al. (1997), since the given time of observation between July 1993 and May 1994 was rather imprecise, but more importantly the separation value of 5.2 ± 0.025 arcsec was in quite good agreement with our measurements, while the position angle of $145.5 \pm 0.5°$ is more than 20° from our measurements and the measurement of Ghez et al. (1997), taken possibly within the same year. According to Ghez et al. (1997), there is also a wide visual companion candidate at 12.5 arcsec separation, although this companion was outside the field of view (FoV) of our NACO S13 observations. Interestingly, Melo (2003) list SZ Cha as a spectroscopic single star, while Reipurth et al. (2002) list it as a good candidate for a PMS spectroscopic binary with a five-day period. Finally, we note that our mean brightness value of SZ Cha B of Ks = 11.22 mag is closely consistent with that of a spectral type M5 star in Cha I, as given by Kraus & Hillenbrand (2007).

WX Cha

Only one epoch was observed by us. To be able to derive relative astrometric results, we re-reduced the data of Lafrenière et al. (2008), and show in Figs. 2 and A.12 all four PMDs. The background star hypothesis is excluded with high significance. From our relative photometry on 2006 March 25 (Table 8), we find the difference in Ks to be approximately 0.4 mag larger than in the H band, leading to the interesting result that WX Cha A seems to be redder than WX Cha B. This could for example be

evidence of an edge-on disk around the secondary, actually being the primary, as found by us in the case of the very young star [MR81] Hα 17 in Corona Australis (Neuhäuser et al. 2009). Moreover, we see a strong variation in the *Ks* band photometry between the data by Lafrenière et al. (2008), rereduced by us, and our data.

WY Cha

As in the case of WX Cha, we obtained a second epoch of relative astrometric measurements by re-reducing the data of (Lafrenière et al. 2008, Fig. A.13). There could be marginal indications of orbital changes in the position angle (1.2σ level). As in the case of WX Cha, we also see from our photometry (Table 8) that WY Cha A seems to be redder than WY Cha B by quite a large amount. In this case, we even saw the effect twice between *H* and *Ks* bands on 2006 March 25 and between *J* and *Ks* bands on 2008 February 20. Moreover, we see a strong variation in the *Ks* band photometry between the dates. Near-infrared photometry with AO of both components as in the case of [MR81] Hα 17 in Corona Australis (Neuhäuser et al. 2009) could either confirm or reject this assumption for WY Cha as well as WX Cha. In addition, Kraus & Hillenbrand (2007) published an ultrawide visual companion candidate at an approximately 28 arcsec separation outside the FoV of our NACO S13 observations.

4.3. Binaries with indications of orbital motion

We present here binaries for which we found significant slopes in the PMDs, probably corresponding to orbital motion. In many cases, however, the evidence is still tentative, requiring confirmation by additional observations.

RX J0915.5-7609

For this star, we adopt a distance of 168 pc (Sartori et al. 2003) and an age of 1.3 Myr (Wahhaj et al. 2010). Since we observed during two epochs, we can give a relative PMD (Fig. A.1). This excludes the background hypothesis with high significance. The early observation of Köhler (2001) suggests that there is a curved orbital motion in the separation (but not in position angle). The observed linear slope in the absolute position angle PMD is consistent with a possible orbital period of the order of 140 years.

RX J0935.0-7804

Our measurement at JD 2 454 515.1 refers to a weighted mean of observations in two band passes, *J* and *Ks*, each one calibrated independently with corresponding HIP 73357 frames. The absolute, as well as the relative PMDs (Fig. A.3) exclude the background hypothesis and reveal rather strong linear orbital displacements in both separation and position angle. This system also seems to be very young with an age estimate of 1.1 Myr (Wahhaj et al. 2010). The observed linear slope in the absolute position angle PMD is consistent with a possible orbital period of the order of 550 years. Since the separation changes for both absolute and relative values almost as much as expected for a maximum change in a circular edge-on orbit, the PA should not change, if edge-on and circular. However, the PA also changes, hence the orbit might be either eccentric or inclined.

RXJ 1014.2-7636

There are rather strong variations in the separation and position angle. The relative PMD (Fig. A.5) in position angle indicates a significantly non-circular orbit, a quite inclined orbit, or a strongly curved orbit because its sign is the opposite of that in the early observation of Köhler (2001). According to Alcala et al. (1997), this is a very young star of spectral type M2 at an age of 0.24 ± 0.29 Myr. For this star, we could not find a convincing distance value in the literature. Although the higher proper motion found for this star (Table 4) indicates that it is close to the Sun, as does the quite high orbital motion found (Tables 6 and 7), the object might not be as close as the distance 14 pc given in Riaz et al. (2006). This is particularly true because it is unlikely that a very young (see above) star will be found in the solar neighbourhood. The amount of orbital motion is still consistent with the distance to Cha I of 165 pc. The slope in the (more long-term) absolute PMD of the position angle is consistent with an orbital period of the order of 190 years. However, the relative PMD indicates that there is a significant position angle difference between the latest two measurements, with a sign that is the opposite of that of the long-term trend. This could be an indication of a curved orbit.

Ced 110 IRS 2

Data for this companion was published for the first time by Lafrenière et al. (2008), although we (Table 9) also imaged this system 37 days before the measurements of Lafrenière et al. (2008). While it had already been found to be a visual binary, we waited for a second epoch of data before presenting here for the first time the high significance of a common proper motion. The background hypothesis can be excluded from the separation behaviour, but not from that of the position angle. On the other hand, there is a significant temporal variation in the position angle of absolute and relative astrometric measurements, but only a marginal variation in the relative separation PMD (Fig. A.7). In addition, Kraus & Hillenbrand (2007) published an ultrawide visual companion candidate displaying an approximately 22 arcsec separation outside the FoV of our NACO S13 observations. The slopes in the PMDs of the position angle are consistent with an orbital period of the order of 120 years.

Cha Hα 2

The binary nature of this object was suggested by Neuhäuser et al. (2002) from HST data. Our two epochs of data are complemented by an archival observation previously discussed in Schmidt et al. (2008b), where we confirm the very close binary nature of the object and derive the masses of both components of the order of 0.1 $M_\odot$, near the lower stellar mass limit, with error bars down to 0.07 $M_\odot$ for one of the components. The components of Cha Hα 2 are among the faintest and least massive member stars found in the Cha star-forming region and one is still a candidate brown dwarf. The absolute PMDs (Fig. A.8) were presented in Schmidt et al. (2008b); here we add an older measurement from Neuhäuser et al. (2002) to the regular PMD (see Fig. 3) after slightly improving the astrometric reduction quality of the original presented data. In addition, we also present the relative PMDs that confirm the linear orbital motion in the separation found in Schmidt et al. (2008b). The position angle does not show significant orbital variations, but it excludes the background hypothesis, confirms the co-moving nature of the components of Cha Hα 2, and indicates that the orbit is edge-on.

RX J1109.4-7627

There are small variations in the separation but a rather strong slope in the position angle, which is consistent with a circular

Table 9. Absolute astrometric results.

Object	JD – 2 446 000 [days]	Ref.	Separation [arcsec] $\rho \pm \delta_\rho$	Sign.[a] not Backg. $\sigma_{\rho,\mathrm{back}}$	Sign. orb. motion $\sigma_{\rho,\mathrm{orb}}$	PA[b] [°] PA $\pm \delta_{\mathrm{PA}}$	Sign.[a] not Backg. $\sigma_{\mathrm{PA,back}}$	Sign. orb. motion $\sigma_{\mathrm{PA,orb}}$
RX J0915.5-7609								
AB	4172.50000	1	0.111 ± 0.007	16	3.1	292.5 ± 4.3	0.5	7.1
	8161.53412		0.1489 ± 0.0031	6.9	1.6	262.763 ± 1.412	5.3	1.5
	8881.59508		0.1385 ± 0.0055	[c]	[c]	259.287 ± 1.920	[c]	[c]
RX J0919.4-7738								
AaB	8515.51911		8.9727 ± 0.1357			194.218 ± 1.400		
AbB	8515.51911		8.9351 ± 0.1352			194.858 ± 1.400		
(AaAb)B[d]	925.53114	2	9.020 ± 0.050	12	0.4	192.350 ± 0.740	7.1	1.3
	2348.81400	3	9.0250 ± 0.0051	10	0.5	194.154 ± 0.036	5.7	0.2
	5549.68730	4	8.9907 ± 0.0881	4.5	0.2	194.396 ± 0.797	2.6	0.1
	8515.51911		8.9567 ± 0.1355	[c]	[c]	194.487 ± 1.400	[c]	[c]
AaAb	4172.50000	1	0.109 ± 0.003	43	0.4	173.9 ± 1.2	29	21
	8515.51911		0.1070 ± 0.0035	[c]	[c]	125.175 ± 2.008	[c]	[c]
RX J0935.0-7804								
AB	4173.50000	1	0.360 ± 0.003	21	8.0	353.9 ± 0.2	16	5.5
	8161.59183		0.4114 ± 0.0059	9.6	0.8	346.840 ± 1.328	5.0	0.6
	8515.10153		0.4146 ± 0.0048	6.2	0.5	346.215 ± 1.009	3.3	0.3
	8882.58189		0.4189 ± 0.0067	[c]	[c]	345.630 ± 1.483	[c]	[c]
RX J0952.7-7933								
AB	4173.50000	1	0.267 ± 0.003	13	2.7	314.6 ± 0.5	12	15
	8160.58336		0.2852 ± 0.0043	7.4	0.4	296.912 ± 1.356	4.2	3.6
	8514.65391		0.2838 ± 0.0032	6.9	0.2	295.658 ± 1.033	3.8	3.3
	8881.63897		0.2818 ± 0.0048	4.8	0.1	293.627 ± 1.498	2.3	2.0
	9250.53614		0.2805 ± 0.0047	2.8	0.3	291.421 ± 1.565	1.2	1.0
	9553.86365		0.2819 ± 0.0050	0.7	0.1	289.616 ± 1.633	0.2	0.2
	9645.57285		0.2826 ± 0.0050	[c]	[c]	289.222 ± 1.653	[c]	[c]
RX J1014.2-7636								
AB	4174.50000	1	0.091 ± 0.007	22	19	259.6 ± 6.5	5.8	4.4
	9250.56298		0.2392 ± 0.0041	14	1.9	291.248 ± 1.571	1.0	0.9
	9645.60036		0.2510 ± 0.0045	[c]	[c]	289.085 ± 1.654	[c]	[c]
SZ Cha								
AB	3476.50000	5	5.3 ± 0.2	2.0	0.8	121 ± 2	1.6	0.9
	5101.55583	6	5.118 ± 0.012	2.0	0.0	123.00 ± 0.15	1.0	0.2
	7782.64912		5.1151 ± 0.0685	0.5	0.0	123.264 ± 1.236	0.2	0.0
	7821.89696	6	5.122 ± 0.0146	0.7	0.0	122.9 ± 0.6	0.4	0.2
	8881.66756		5.1189 ± 0.0819	[c]	[c]	123.258 ± 1.481	[c]	[c]
Ced 110 IRS 2								
AB	7782.61949		0.1481 ± 0.0027	8.7	1.1	128.196 ± 1.428	0.3	2.6
	7819.92133	6	0.140 ± 0.0063	4.7	0.4	126.1 ± 2.8	0.6	1.2
	8515.61187		0.1427 ± 0.0039	[c]	[c]	121.952 ± 1.888	[c]	[c]
Cha Hα 2								
AB	5843.40756	7,8	0.21 ± 0.05	0.1	1.0	37.6 ± 6.4	2.9	0.6
	7454.63563	7,9	0.1652 ± 0.0037	1.0	1.3	40.121 ± 1.871	2.1	0.5
	7782.68981	7	0.1667 ± 0.0031	1.5	1.9	40.875 ± 1.436	2.0	0.2
	8160.71934	7	0.1591 ± 0.0026	[c]	[c]	41.250 ± 1.402	[c]	[c]
VW Cha								
AB	7783.90711		0.6491 ± 0.0087			178.929 ± 1.236		
AC	7783.90711		0.7153 ± 0.0096			185.324 ± 1.236		
A(BC)[e]	2630.83699	10	0.69 ± 0.01	1.6	1.3	178.7 ± 3.2	6.9	0.8
	3468.50000	5	0.66 ± 0.03	1.7	0.4	184 ± 2	6.5	1.1
	3490.53749	11	0.72 ± 0.03	0.6	1.5	178.6 ± 1.0	9.8	1.8
	5230.38638	12,13	0.6592 ± 0.0253	1.2	0.6	178.001 ± 0.405	10	2.6
	5615.50000	14	0.683 ± 0.008	0.5	0.9	179.4 ± 0.7	8.4	1.4
	6690.70028	15	0.6770 ± 0.0011	0.2	0.5	180.076 ± 0.483	5.5	1.0
	7783.90711		0.6722 ± 0.0090	[f]	[f]	181.404 ± 1.236	[f]	[f]
	7821.93038	6	0.6749 ± 0.0025	0.2	0.3	181.148 ± 0.581	0.2	0.2
BC	5615.50000	14	0.100 ± 0.006	9.3	0.1	233.3 ± 3.3	2.8	0.6
	6690.70028	15	0.113 ± 0.001	6.7	7.1	232.9 ± 0.5	3.1	1.3
	7783.90711		0.1008 ± 0.0014	[f]	[f]	231.136 ± 1.238	[f]	[f]
	7821.93038	6	0.100 ± 0.0012	0.4	0.4	231.0 ± 0.8	0.3	0.1
RX J1109.4-7627								
AB	7820.51080	16	0.0806 ± 0.0018	0.8	2.3	85.733 ± 1.376	3.4	10.1
	8882.81186		0.0792 ± 0.0020	3.1	1.8	70.222 ± 1.708	2.1	3.2

Table 9. continued.

Object	JD – 2 446 000 [days]	Ref.	Separation [arcsec] $\rho \pm \delta_\rho$	Sign.[a] not Backg. $\sigma_{\rho,\mathrm{back}}$	Sign. orb. motion $\sigma_{\rho,\mathrm{orb}}$	PA[b] [°] PA $\pm \delta_{\mathrm{PA}}$	Sign.[a] not Backg. $\sigma_{\mathrm{PA,back}}$	Sign. orb. motion $\sigma_{\mathrm{PA,orb}}$
	9251.69870		0.0736 ± 0.0024	[c]	[c]	62.006 ± 1.914	[c]	[c]
HD 97300								
AB	3468.50000	5	0.84 ± 0.04	1.9	1.4	327 ± 2	5.9	0.2
	7820.90105	16	0.7855 ± 0.0106	0.8	0.2	326.994 ± 1.246	1.5	0.3
	8160.60766		0.7827 ± 0.0112	0.4	0.0	326.908 ± 1.320	0.8	0.2
	8516.71442		0.7819 ± 0.0118	[c]	[c]	326.489 ± 1.250	[c]	[c]
WX Cha								
AB	3473.50000	5	0.79 ± 0.04	5.1	1.0	55 ± 2	6.1	1.0
	7819.89102	16	0.7464 ± 0.0106	3.2	0.0	52.169 ± 1.275	1.5	0.2
	8881.91858		0.7467 ± 0.0120	[c]	[c]	52.502 ± 1.482	[c]	[c]
WY Cha								
AB	7819.63848	16	0.1241 ± 0.0033	7.5	0.4	241.737 ± 1.474	2.8	0.5
	8516.70106		0.1227 ± 0.0019	[c]	[c]	240.775 ± 1.407	[c]	[c]
HJM C 7-11								
AB	3476.50000	5	1.2[g] ± 0.1	5.2	10[g]	336 ± 5	7.1	0.8
	7819.57870	16	0.1772 ± 0.0041	6.3	0.6	334.781 ± 1.440	7.7	1.4
	8161.78979		0.1774 ± 0.0044	4.9	0.6	333.033 ± 1.788	5.6	0.5
	8515.79485		0.1748 ± 0.0032	3.8	0.1	332.639 ± 1.542	4.1	0.4
	8881.70578		0.1744 ± 0.0029	[c]	[c]	331.856 ± 1.491	[c]	[c]
Sz 41								
AB	3476.50000	5	1.5 ± 0.8	0.4	0.6	150 ± 20	1.4	0.6
	6661.86278	15	1.974 ± 0.002	2.6	0.1	162.4 ± 0.5	3.7	0.3
	7819.54463	16	1.9720 ± 0.0266	1.2	0.1	162.737 ± 1.245	1.8	0.1
	8619.97904	12	1.9623 ± 0.0169	0.1	0.4	162.200 ± 0.193	1.4	0.4
	8881.88546		1.9760 ± 0.0316	0.3	0.0	162.685 ± 1.482	0.5	0.1
	9250.08623		1.9767 ± 0.0334	[c]	[c]	162.862 ± 1.564	[c]	[c]
HM Anon								
AB	3470.50000	5	0.27 ± 0.03	9.6	0.9	236 ± 5	6.2	2.3
	7820.86777	16	0.2469 ± 0.0033	9.1	1.0	246.743 ± 1.245	4.8	0.6
	8234.48285	16	0.2455 ± 0.0036	6.0	0.7	247.312 ± 1.338	2.5	0.3
	8515.69528		0.2440 ± 0.0037	3.9	0.4	247.635 ± 1.401	1.9	0.2
	8882.87337		0.2419 ± 0.0039	[c]	[c]	247.991 ± 1.483	[c]	[c]

Notes. [(a)] Assuming the fainter component is a non-moving background star. [(b)] Position angle (PA) is measured from N over E to S. [(c)] Significances are given relative to the last epoch. [(d)] Results of component A relative to the centre of brightness (brightness ratio ∼1.37 at *K*s band). [(e)] Results of component A relative to the centre of brightness (brightness ratio ∼1.75 at *K*s band as well as to the centre of mass (masses from apparent magnitudes, Table 7, and distance of Chamaeleon cloud of 165 ± 30 pc, using the models of Baraffe et al. (1998), giving for B 0.37 $M_\odot$ and for C 0.21 $M_\odot$ at 1 Myr, resulting in approximately the same ratio of ∼1.76 as the brightnesses) of components B and C. [(f)] Significances are given relative to the second to last epoch. [(g)] Included as given in Ghez et al. (1997), this might be a typo, being actually 0.2 arcsec.

References. (1) Köhler (2001); date given, assuming midnight for calculation of JD. (2) Sinachopoulos (1988). (3) Calculated from the HIPPARCOS catalogue (Perryman et al. 1997) position and positional error at the catalogue epoch (J1991.25). (4) Calculated from the 2MASS catalogue (Skrutskie et al. 2006) position and positional error. (5) Ghez et al. (1997); date given, assuming midnight for calculation of JD. (6) Lafrenière et al. (2008). (7) Schmidt et al. (2008b), improved. (8) Neuhäuser et al. (2002). (9) see also Ahmic et al. (2007) and Lafrenière et al. (2008). (10) Brandner (1992). (11) Brandner et al. (1996). (12) HST data from ESO/ST-ECF science archive, only position measurement error in RA and Dec considered. (13) From ESO/ST-ECF science archive, see also Stapelfeldt (2001), Padgett & Stapelfeldt (2001). (14) Brandeker et al. (2001); date given, assuming midnight of central of three observing days for calculation of JD. (15) Correia et al. (2006). (16) Rereduced, see also Lafrenière et al. (2008).

pole-on orbit of a period of the order of 62 years. The relative and absolute PMDs (Fig. A.10) are almost identical in this case, owing to the lack of earlier observations and the small separation of the components, reducing the influence of the more imprecise absolute astrometric calibration.

HD 97300

This is the most massive binary of our sample with a spectral type B9V (Rydgren 1980; Gürtler et al. 1999). For this star, we adopt a distance of 179 pc (van Leeuwen 2007) and an age of 5.6 ± 2.0 Myr (Tetzlaff et al. 2011). Two epochs were observed by us. In addition, we re-reduced the data of Lafrenière et al. (2008) in order to be able to include this epoch in our relative PMDs (Fig. A.11). There is a quite significant linear orbital motion in both of the separation PMDs, as well as in the relative astrometric measurements of the position angle. The background hypothesis is rejected with high significance in all diagrams.

HJM C7-11

We consider the strongly deviating value of the early separation measurement of 1.2 arcsec by Ghez et al. (1997) as a misprint, as it might mean 0.2 arcsec. Disregarding this value, we obtain a co-moving pair with a rather constant separation, but slight indications of a position angle slope (Fig. A.14). A circular pole-on orbit would have a period of the order of 500 years. While Torres et al. (2006) give a multiplicity flag of "SB?" (spectroscopic

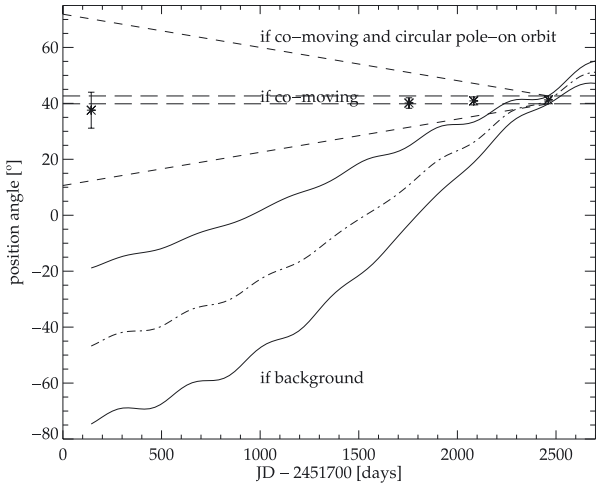

Fig. 3. Proper motion diagram (PMD) from absolute astrometric measurements for the position angle in the Cha Hα 2 AB system. See text for more information.

binary), this possibility was not mentioned in other publications (Covino et al. 1997; Joergens 2006). In addition, Kraus & Hillenbrand (2007) published an ultrawide visual companion candidate at an approximately 13.6 arcsec separation outside the FoV of our NACO S13 observations.

Sz 41

An early observation is available of the 4 Myr (Wahhaj et al. 2010) old star (Ghez et al. 1997) that is of very low precision. This and all remaining observations are consistent with a co-moving binary without any significant orbit evidence in separation. The position angle change for relative astrometric measurements might either indicate orbital motion or a 2σ outlier of our first own measurement. The point from the re-reduced data of Lafrenière et al. (2008) is consistent with no orbital motion at all, although it does have a larger time difference and hence, larger error bars due to the possible larger amount of orbital motion of the calibration binary. The background hypothesis is ruled out with high significance, especially according to the relative PMD (Fig. A.15), which contains three epochs. According to Brandner (1992) and Reipurth & Zinnecker (1993), there is a second wide visual companion candidate at 11.4 arcsec separation outside the FoV of our NACO S13 observations. Reipurth et al. (2002) report from their spectroscopy data, with the primary and secondary situated in the spectrograph entrance window, that the object is a spectroscopic binary candidate with a possible period of about 125 days. While the spectro-astrometric displacement found by Takami et al. (2003) is small and might be caused by the binarity also recovered by us at ~2 arcsec, Covino et al. (1997), Melo (2003), Guenther et al. (2007) and Joergens (2008) all found no evidence of a spectroscopic binarity.

HM Anon

In addition to our two epochs of data we re-reduced the data of Lafrenière et al. (2008) in order to be able to include these epochs in our relative PMD (Fig. A.16). All diagrams reveal that there are significant linear orbital motions in separation and position angle, and enable us to reject the background hypothesis with large significance. As given in Skiff (2009), the Tycho-2 coordinates are incorrect and HM Anon can be identified with TYC 9414-1250-1. Since the proper motion of Tycho-2 (Høg et al. 2000) differs greatly from the mean value for Cha I (Luhman et al. 2008), we chose to use the value of UCAC 3 (Zacharias et al. 2010); this is because this measurement is consistent with the Cha I median value (see Table 4), although UCAC 3 found fewer than two good matches, while including the catalogues used for Tycho-2. HM Anon is the only object in our sample for which we could find values of the orbital motion in the literature (Woitas et al. 2001). If we convert their units ($\mathrm{km\,s^{-1}}$) into those of our Table 6 (mas/yr), using the distance to Cha I of 160 pc as assumed there and given in Wichmann et al. (1998) and from $\mathrm{km\,s^{-1}}$ to °/yr assuming the same distance and a separation of the components of 245 mas, we derive the trends of -3.5 ± 9.8 mas/yr in separation and 4.1 ± 4.0°/yr in position angle observed by Woitas et al. (2001), consistent with our new, more precise values listed in Table 6. As discussed for RX J0935.0-7804, the orbit of this binary might be inclined and/or eccentric.

4.4. Triples and quadruples

RX J0919.4-7738

For this star, we adopt a distance of 56.8 ± 2.8 pc (van Leeuwen 2007) and an age of 16.1 ± 2.5 Myr (Tetzlaff et al. 2011), consistent with the earlier value of 14 Myr given by Neuhäuser & Brandner (1998). This is a strong quadruple system candidate. It consists of a wide binary (separation 9 arcsec) whose southern component is a double-lined spectroscopic binary (Covino et al. 1997) called B, while the northern component is visually double, beeing resolved for the first time by Köhler (2001) called Aa/Ab. Our observations comprise only one epoch of Aa/Ab/B, therefore no relative PMDs can be obtained. We used the catalogues of Hipparcos (Perryman et al. 1997) and 2MASS (Skrutskie et al. 2006; Cutri et al. 2003) in order to derive separations and position angles between Aa/Ab and B, using the centroid in magnitude for Aa/Ab (which were not resolved by Hipparcos and 2MASS). These data do not reveal significant variations in either the separation or position angle of the wide binary, and their PMD is consistent with a co-moving binary (Fig. 4). The PMD of the Aa/Ab pair (Fig. A.2) shows strong variability in the position angle, while the distance seems to be constant during the time interval of about 4300 days between the two observations available at present. This is consistent with a co-moving binary in a circular pole-on orbit, with an orbital period of the order of 90 years. We did not include in our analysis the position values of Mason et al. (1998), Tokovinin et al. (2010), and the earlier ones as in Torres (1986), noting that there has been little or no change in the orbit of the wide binary since 1872, as no error bars are given for the separation and position angle. For a further discussion of the system, we refer to Desidera et al. (2006) and Tokovinin et al. (2010).

RX J0952.7-7933

For this star, we adopt an age of 3 Myr, since Frink et al. (1998) give this value for their subgroup 1 of stars, mentioning that RX J0952.7-7933 might be a member of this subgroup judging from its proper motion alone, while warning that the reflex motion of the sun is very similar to the typical proper motion of Chamaeleon member stars. The object is a spectroscopic triple star (Covino et al. 1997), partly resolved by Köhler (2001) and us here, although we are unable to judge from the currently available data which resolved star of the components is the additional spectroscopic binary. Components A and B are co-moving with

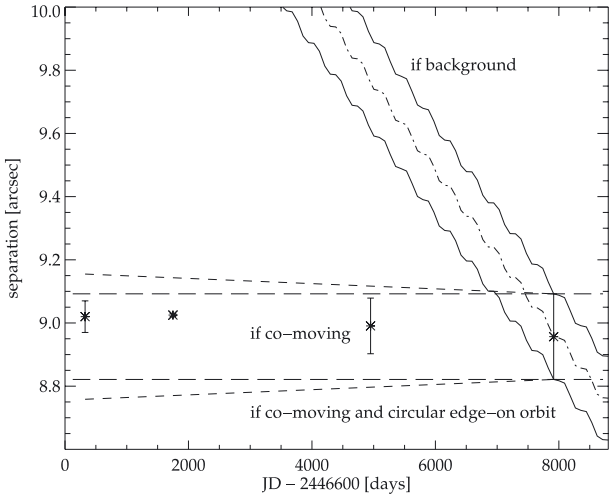

Fig. 4. Proper motion diagram (PMD) from absolute astrometric measurements for the separation in the RX J0919.4-7738 AaAbB system. See text for more information.

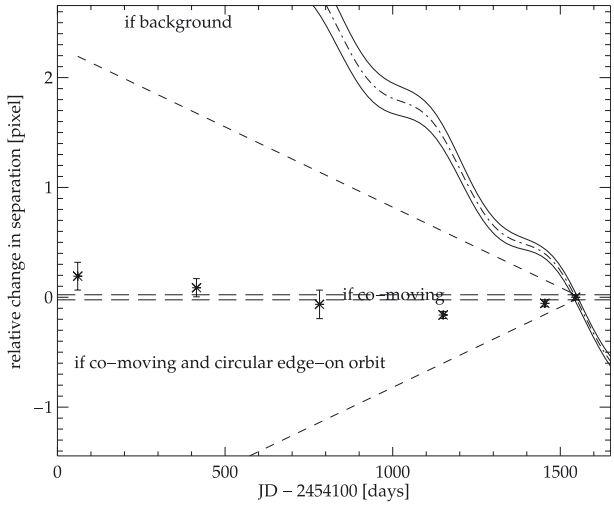

Fig. 5. Proper motion diagram (PMD) from relative astrometric measurements for the separation in the RX J0952.7-7933 AB system. See text for more information.

only marginal variations in the separation: the six data points in the relative separation PMD could reveal some indication of an orbital curvature for the triple system AB. This curvature is strongly consistent with a first astrometric detection of the third component of the spectroscopic triple, having in this case an orbital period of approximately five years. On the other hand, there is a rather strong slope in both of the position angle PMDs (Fig. A.4), which is consistent with a circular pole-on obit of the wide binary and a period of the order of 200 years.

VW Cha

This object was recognized as a binary by Brandner (1992). Additional measurements were published by Ghez et al. (1997) and Brandner et al. (1996) and were found in the ESO/ST-ECF science archive (see also Stapelfeldt 2001; Padgett & Stapelfeldt 2001, for more information on the observations with the HST). Brandeker et al. (2001) resolved, for the first time, the southern component of the original binary into two stars, now called B/C. Consequently, the triple system was measured by Correia et al. (2006) and Lafrenière et al. (2008), as well as in one epoch by us (therefore no relative PMD is available). Figures 6 and A.9 show the PMDs of A versus (vs.) B/C and B vs. C. The position angle variations in the former PMD are consistent with a circular pole-on orbit, excluding the background hypothesis, while the separation values do not allow firm conclusions. The B/C pair is bound, and the three points in the separation PMD could indicate curved orbital motion. Reipurth & Zinnecker (1993) and Correia et al. (2006) found evidence of a possible fourth component in this system, outside the field of our NACO observations at 16.7 arcsec separation. VW Cha was found to be spectroscopically multiple by Melo (2003) and Torres et al. (2006), although according to the details in the discussion of Melo (2003) the three found components might in fact be the three resolved inner components by Brandeker et al. (2001).

5. Conclusions

Our astrometric results from VLT NACO observations based on new data of one to five epochs confirm the physical connection of the secondary stars in all (previously known, but hitherto unconfirmed) 16 binary and multiple members of the star-forming region in Chamaeleon. The angular separation between the components range from 0.07 to 9.0 arcsec (Table 9), corresponding to projected minimum distances of between 6 and 845 AU (Table 6). All secondary components are brighter than 11.5 mag in the Ks band (Table 8), despite our observations reaching limiting magnitudes that vary between 16.5 and 18 mag in Ks. On average, we expect only 0.117 stars per field, according to 2MASS (cf. Table 1). However, only about 7 % of all 2MASS stars in our statistics are as bright as $K \leq 11.5$ mag, therefore the probability of a chance coincidence at this brightness level ranges between 0.4% and 1.2%, according to the different star densities in our fields. Statistically, we should observe about 125 different fields, in order to expect one chance coincidence of a star brighter than 11.5 mag with one of our targets. Therefore, it is unsurprising that background stars in our small NACO fields are missing.

However, from a statistical point of view, there is an additional strong argument for a true physical connection between most components of our targets: In only two fields are the angular separations larger than 5 arcsec (RX J0919.4-7738 and SZ Cha), i.e. of the same order of magnitude as our NACO field size. There is one additional case (Sz 41) with a separation of 1.9 arcsec, but in all the other 13 cases the components are closer than 1 arcsec. Therefore, a realistic estimation of a chance coincidence is still much lower than the above value.

On the other hand, we should emphasize that, in principle, a real proof of a gravitational bond between the components is only given, if curvature in the orbit can be measured (which would have to also differ from a hyperbolic ejection orbit). Marginal indications of possible curvatures are found in four targets (RX J0915.5-7609, RX J0952.7-7933, RX J1014.2-7636, and VW Cha). Future observations should confirm this and improve the orbital parameters. We also refer to Neuhäuser et al. (2010) and Mugrauer et al. (2010) for further detailed discussions and sub-stellar examples of the first indications of orbital curvature. As an alternative explanation of apparently co-moving binaries, we could suppose that we have seen two seperate members of the star-forming region in Chamaeleon, aligned by chance along our line of sight. Our orbital motions of a few to several mas/yr (Tables 6 and 7) would be typical of the velocity dispersion in star-forming regions such as Cha I (Ducourant et al. 2005). However, the aforementioned statistical arguments do not support this idea. We therefore have observed,

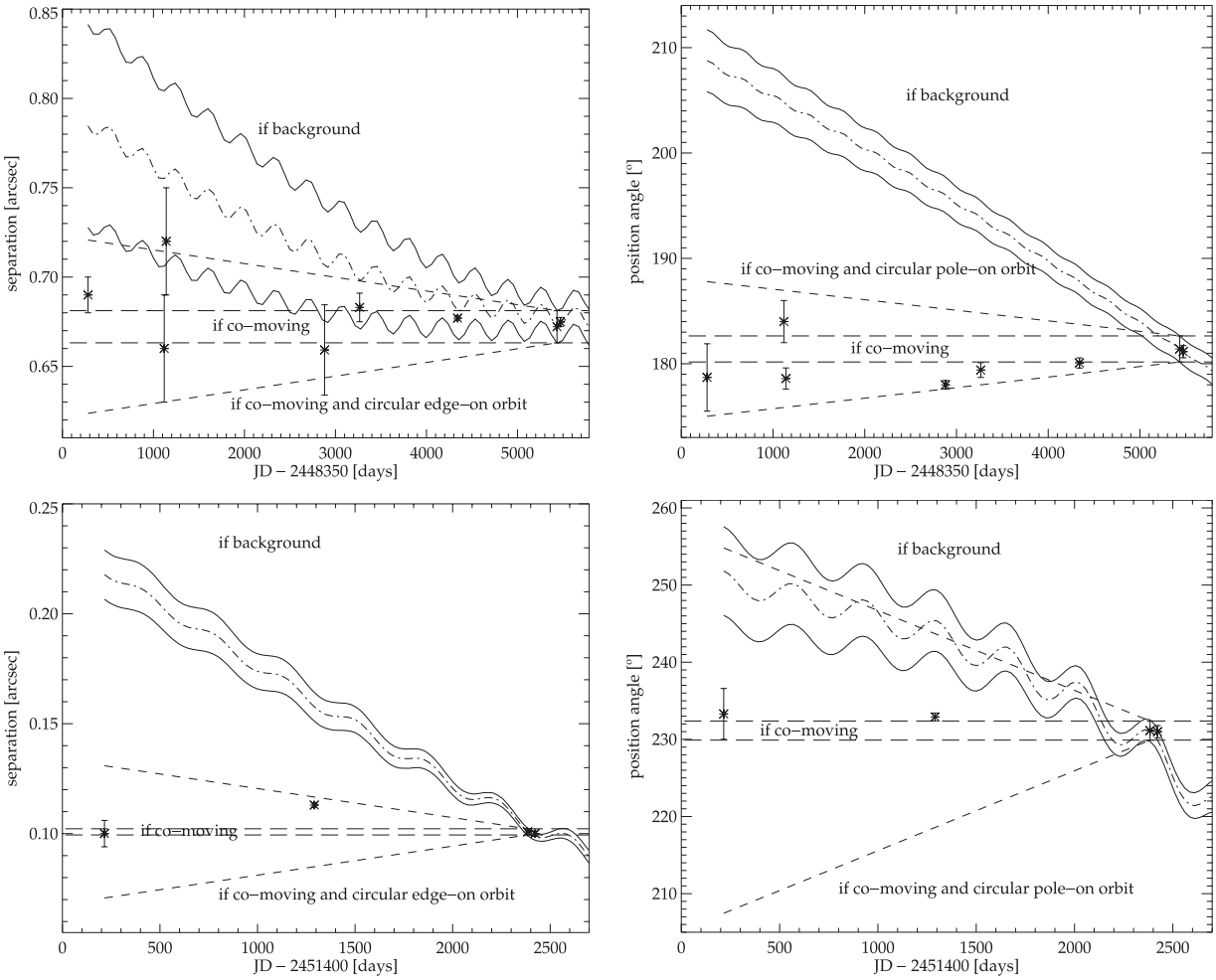

Fig. 6. Proper motion diagrams (PMD) from absolute astrometric measurements (*top*) for separation and position angle change (*left to right*) of VW Cha A relative to the centroid of B & C and from absolute astrometric measurements (*bottom*) for separation and position angle change (*left to right*) of VW Cha B relative to VW Cha C. See text for more information.

with very high probablilty, 16 physically bound binaries or multiple systems. Even if one turns out to be an unbound case of two young Chamaeleon members, the age and distance (within the given uncertainties) would be the same for both objects, and likewise the masses of these individual Chamaeleon member objects.

The 2MASS catalogue separates the components only for the two cases with separations ≥5 arcsec mentioned above, in all other cases the positions and magnitudes in 2MASS refer to the combined light (cf. Sect. 3). The limiting magnitude of 2MASS is near $K = 16$ mag, far below the limit of the faintest secondary components investigated in this paper ($K = 11.5$ mag, see Table 8). Might we be missing additional low-mass components of larger separations, outside of our NACO field of view? To investigate this possibility, we searched in the 2MASS catalogue for additional components at angular distances of up to 20 arcsec, around all 16 targets presented here, as well as around CT Cha (Schmidt et al. 2008a). This search revealed a total of 17 candidate stars, i.e. on average 1.0 stars per field, with separations ranging between 7.5 and 16.5 arcsec. Since these search fields are 6.83 times larger than the FoV of NACO, we expect on average about $0.117 \cdot 6.83 = 0.8$ stars per field, very close to the observed number. Assuming that we can also detect objects in the additional amount of field created by the jittering procedure, in spite of the fact that we cannot search as deeply in this additional field as in the inner part of the image, we find that the 2MASS search fields are only 5.2 times larger than the NACO FoV plus two arcsec of the four arcsecond jitter box width used. With this assumption, we thus expect to detect approximately 0.61 stars per field.

On average, we found 0.2–0.39 objects too many in the search areas per star or in total 3.4–6.6 candidate stars that could be additional multiple-star components. Moreover, there is a large excess of bright stars: a total of 4 candidate stars (=24%) are in the range $K < 11.99$ mag, while our 2MASS counts reveal that only 9 % of all stars are in this brightness range. A similar excess is present in the magnitude range $12.0 < K < 13.99$ mag in which we found 6 stars (=35%), but expect only 19%. Consequently, there is a deficit of the faintest stars $K > 14.0$ mag (7 stars = 41% observed, but 72% expected), of faint background stars behind the dark cloud. According to these results, a total of 5–6 candidate stars with $K < 14.0$ mag could be additional multiple star components of our targets.

The given magnitude limit of $K = 11.5$ mag of our target stars has already been mentioned. It correponds at the distance of the Cha I region rather precisely to the mass limit of 0.08 $M_\odot$ of hydrogen burning stars. We should emphasize that this limit is only reached by one binary star (Cha Hα 2, see also Schmidt et al. 2008b), both of whose components are very near to this lower limit of possible stellar masses, one of them still being a brown dwarf candidate. SZ Cha B is the only other star with $K > 11$ mag, while all the remaining targets of our sample

contain much brighter components with $K \leq 10.6$ mag, corresponding to a mass of 0.16 $M_{\odot}$ at the average age (2 Myr) and the distance of Cha I (165 pc) using the Baraffe et al. (1998) models. In contrast to many studies (Tokovinin 2000; Halbwachs et al. 2003), we find that binary or multiple systems with relatively massive primary components tend to avoid the simultaneous formation of equal-mass secondary components (as also found by Mazeh et al. 2003). Extremely low-mass secondary components are hard to find for high and low mass primaries owing to the much higher dynamic range and the faintness of the secondaries.

Acknowledgements. We would like to thank the ESO Paranal Team, the ESO User Support department and all other very helpful ESO services, the anonymous referee for helpful comments and finally the language editor Claire Halliday for corrections. N.V. acknowledges support by Comité Mixto ESO-Gobierno de Chile, as well as by the Gemini-CONICYT fund 32090027. T.O.B.S. acknowledges support from the Evangelisches Studienwerk e.V. Villigst, from the German National Science Foundation (Deutsche Forschungsgemeinschaft, DFG) in grant NE 515/30-1 and from Friedrich Schiller University Jena/State of Thuringia/Germany. A.S. acknowledges support from NSF under grants AST-0708074 and AST-1108860. This publication makes use of data products from the Two Micron All Sky Survey, which is a joint project of the University of Massachusetts and the Infrared Processing and Analysis Center/California Institute of Technology, funded by the National Aeronautics and Space Administration and the National Science Foundation. This research has made use of the VizieR catalog access tool and the Simbad database, both operated at the Observatoire Strasbourg. This reasearch makes use of the HIPPARCOS Catalogue, the primary result of the HIPPARCOS space astrometry mission, undertaken by the European Space Agency. This research has made use of NASA's Astrophysics Data System Bibliographic Services.

References

Ageorges, N., Eckart, A., Monin, J.-L., & Menard, F. 1997, A&A, 326, 632
Ahmic, M., Jayawardhana, R., Brandeker, A., et al. 2007, ApJ, 671, 2074
Alcala, J. M., Krautter, J., Covino, E., et al. 1997, A&A, 319, 184
Baraffe, I., Chabrier, G., Allard, F., & Hauschildt, P. H. 1998, A&A, 337, 403
Baraffe, I., Chabrier, G., Barman, T. S., Allard, F., & Hauschildt, P. H. 2003, A&A, 402, 701
Bertout, C., Robichon, N., & Arenou, F. 1999, A&A, 352, 574
Brandeker, A., Liseau, R., Artymowicz, P., & Jayawardhana, R. 2001, ApJ, 561, L199
Brandner, W. 1992, Ph.D. Thesis, Diplom thesis, Julius-Maximilians-Universität Würzburg
Brandner, W., & Zinnecker, H. 1997, A&A, 321, 220
Brandner, W., Alcala, J. M., Kunkel, M., Moneti, A., & Zinnecker, H. 1996, A&A, 307, 121
Camargo, J. I. B., Ducourant, C., Teixeira, R., et al. 2003, A&A, 409, 361
Chabrier, G., Baraffe, I., Allard, F., & Hauschildt, P. 2000, ApJ, 542, 464
Chauvin, G., Lagrange, A.-M., Bonavita, M., et al. 2010, A&A, 509, A52
Comerón, F., Rieke, G. H., & Neuhäuser, R. 1999, A&A, 343, 477
Correia, S., Zinnecker, H., Ratzka, T., & Sterzik, M. F. 2006, A&A, 459, 909
Covino, E., Alcala, J. M., Allain, S., et al. 1997, A&A, 328, 187
Cutri, R. M., Skrutskie, M. F., van Dyk, S., et al. 2003, 2MASS All Sky Catalog of point sources
Damjanov, I., Jayawardhana, R., Scholz, A., et al. 2007, ApJ, 670, 1337
Desidera, S., Gratton, R. G., Lucatello, S., Claudi, R. U., & Dall, T. H. 2006, A&A, 454, 553
Devillard, N. 1997, The Messenger, 87, 19
Diolaiti, E., Bendinelli, O., Bonaccini, D., et al. 2000, in Proc. SPIE 4007, ed. P. L. Wizinowich, 879
Ducourant, C., Teixeira, R., Périé, J. P., et al. 2005, A&A, 438, 769
Frink, S., Roeser, S., Alcala, J. M., Covino, E., & Brandner, W. 1998, A&A, 338, 442
Ghez, A. M., McCarthy, D. W., Patience, J. L., & Beck, T. L. 1997, ApJ, 481, 378
Guenther, E. W., Esposito, M., Mundt, R., et al. 2007, A&A, 467, 1147
Gürtler, J., Schreyer, K., Henning, T., Lemke, D., & Pfau, W. 1999, A&A, 346, 205
Halbwachs, J. L., Mayor, M., Udry, S., & Arenou, F. 2003, A&A, 397, 159
Hambly, N. C., MacGillivray, H. T., Read, M. A., et al. 2001, MNRAS, 326, 1279
Høg, E., Fabricius, C., Makarov, V. V., et al. 2000, A&A, 355, L27
Hyland, A. R., Jones, T. J., & Mitchell, R. M. 1982, MNRAS, 201, 1095
Joergens, V. 2006, A&A, 448, 655
Joergens, V. 2008, A&A, 492, 545
Köhler, R. 2001, AJ, 122, 3325
Kraus, A. L., & Hillenbrand, L. A. 2007, ApJ, 662, 413
Lafrenière, D., Jayawardhana, R., Brandeker, A., Ahmic, M., & van Kerkwijk, M. H. 2008, ApJ, 683, 844
Lenzen, R., Hartung, M., Brandner, W., et al. 2003, in Proc. SPIE, 4841, 944
Luhman, K. L. 2007, ApJS, 173, 104
Luhman, K. L. 2008, Chamaeleon in Handbook of Star Forming Regions, Vol. II, ed. B. Reipurth (ASP), 169
Luhman, K. L., Allen, L. E., Allen, P. R., et al. 2008, ApJ, 675, 1375
Mason, B. D., Henry, T. J., Hartkopf, W. I., ten Brummelaar, T., & Soderblom, D. R. 1998, AJ, 116, 2975
Mason, B. D., Wycoff, G. L., Hartkopf, W. I., Douglass, G. G., & Worley, C. E. 2001, AJ, 122, 3466
Mazeh, T., Simon, M., Prato, L., Markus, B., & Zucker, S. 2003, ApJ, 599, 1344
Melo, C. H. F. 2003, A&A, 410, 269
Mugrauer, M., Vogt, N., Neuhäuser, R., & Schmidt, T. O. B. 2010, A&A, 523, L1
Neuhäuser, R., & Brandner, W. 1998, A&A, 330, L29
Neuhäuser, R., Brandner, W., Alves, J., Joergens, V., & Comerón, F. 2002, A&A, 384, 999
Neuhäuser, R., Guenther, E. W., Wuchterl, G., et al. 2005, A&A, 435, L13
Neuhäuser, R., Mugrauer, M., Seifahrt, A., Schmidt, T. O. B., & Vogt, N. 2008, A&A, 484, 281
Neuhäuser, R., Krämer, S., Mugrauer, M., et al. 2009, A&A, 496, 777
Neuhäuser, R., Schmidt, T. O. B., Hambaryan, V. V., & Vogt, N. 2010, A&A, 516, A112
Padgett, D. L., & Stapelfeldt, K. R. 2001, BAAS, 33, 1395
Perryman, M. A. C., Lindegren, L., Kovalevsky, J., et al. 1997, A&A, 323, L49
Preibisch, T. 1997, A&A, 320, 525
Reipurth, B., & Zinnecker, H. 1993, A&A, 278, 81
Reipurth, B., Lindgren, H., Mayor, M., Mermilliod, J.-C., & Cramer, N. 2002, AJ, 124, 2813
Riaz, B., Gizis, J. E., & Harvin, J. 2006, AJ, 132, 866
Röser, S., Schilbach, E., Schwan, H., et al. 2008, A&A, 488, 401
Rousset, G., Lacombe, F., Puget, P., et al. 2003, in Proc. SPIE 4839, eds. P. L. Wizinowich, & D. Bonaccini, 140
Rydgren, A. E. 1980, AJ, 85, 444
Sartori, M. J., Lépine, J. R. D., & Dias, W. S. 2003, A&A, 404, 913
Schmidt, T. O. B., Neuhäuser, R., Seifahrt, A., et al. 2008a, A&A, 491, 311
Schmidt, T. O. B., Neuhäuser, R., Vogt, N., et al. 2008b, A&A, 484, 413
Skiff, B. A. 2009, VizieR Online Data Catalog, 1, 2023
Skrutskie, M. F., Cutri, R. M., Stiening, R., et al. 2006, AJ, 131, 1163
Stapelfeldt, K. 2001, in Tetons 4: Galactic Structure, Stars and the Interstellar Medium, eds. C. E. Woodward, M. D. Bicay, & J. M. Shull, ASP Conf. Ser., 231, 620
Takami, M., Bailey, J., & Chrysostomou, A. 2003, A&A, 397, 675
Tetzlaff, N., Neuhäuser, R., & Hohle, M. M. 2011, MNRAS, 410, 190
Tokovinin, A. A. 2000, A&A, 360, 997
Tokovinin, A., Hartung, M., & Hayward, T. L. 2010, AJ, 140, 510
Torres, G. 1986, A&AS, 64, 105
Torres, C. A. O., Quast, G. R., da Silva, L., et al. 2006, A&A, 460, 695
US Government Printing Office (Usgpo) 2003, The Astronomical Almanac for the year 2005
van Leeuwen, F. 2007, A&A, 474, 653
Wahhaj, Z., Cieza, L., Koerner, D. W., et al. 2010, ApJ, 724, 835
Wenger, M., Oberto, A., Bonnarel, F., et al. 2007, in Library and Information Services in Astronomy V, eds. S. Ricketts, C. Birdie, & E. Isaksson, ASP Conf. Ser., 377, 197
Whittet, D. C. B., Prusti, T., Franco, G. A. P., et al. 1997, A&A, 327, 1194
Wichmann, R., Bastian, U., Krautter, J., Jankovics, I., & Rucinski, S. M. 1998, MNRAS, 301, L39
Woitas, J., Köhler, R., & Leinert, C. 2001, A&A, 369, 249
Zacharias, N., Urban, S. E., Zacharias, M. I., et al. 2004, AJ, 127, 3043
Zacharias, N., Finch, C., Girard, T., et al. 2010, AJ, 139, 2184

Pages 17 to 32 are available in the electronic edition of the journal at http://www.aanda.org

Appendix A: Proper motion diagrams (PMDs)

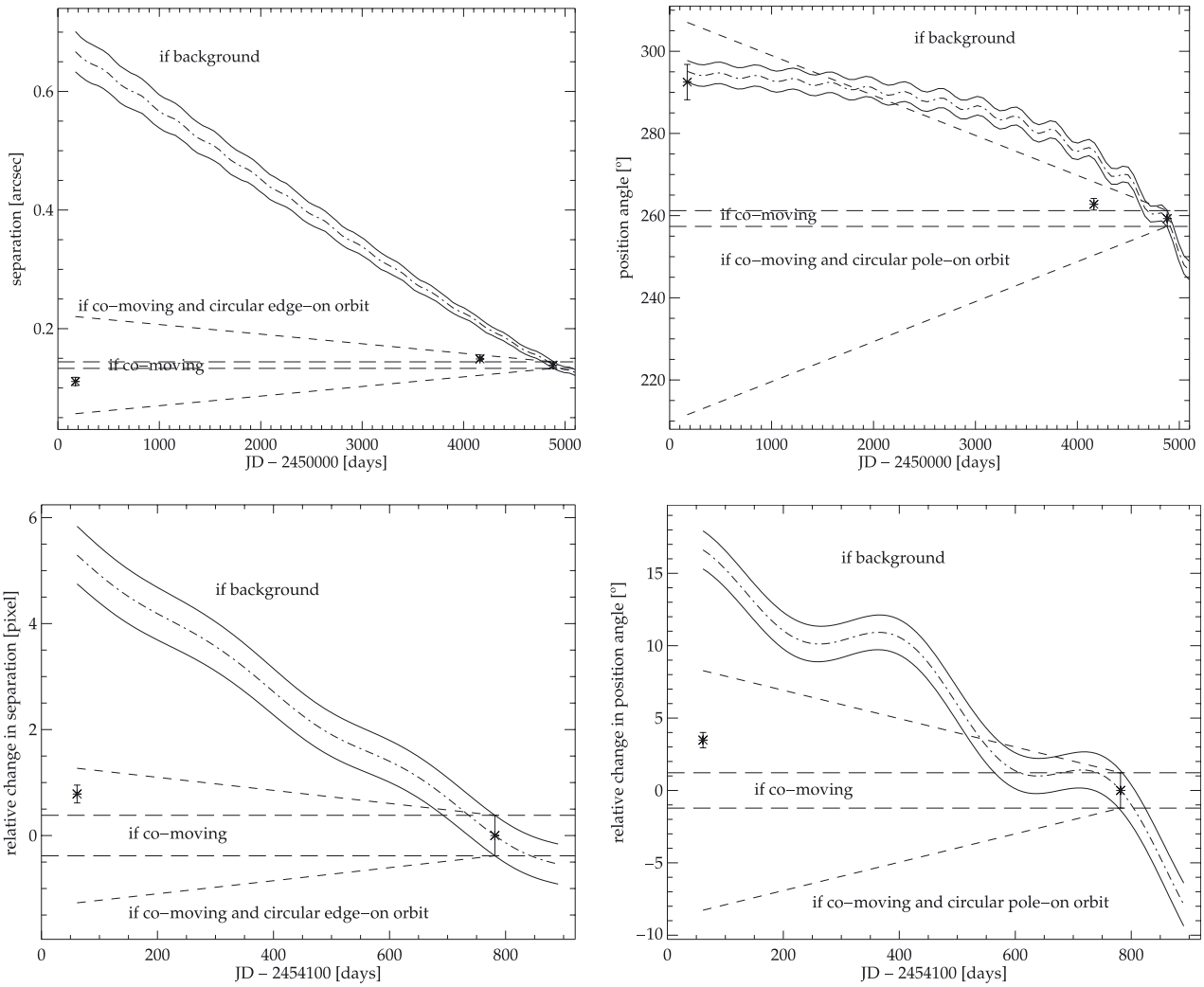

Fig. A.1. Proper motion diagrams (PMD) for separation and position angle change from absolute astrometric measurements (*top*, *left to right*) and from relative astrometric measurements (*bottom*, *left to right*) in the RX J0915.5-7609 AB system. See text for more information.

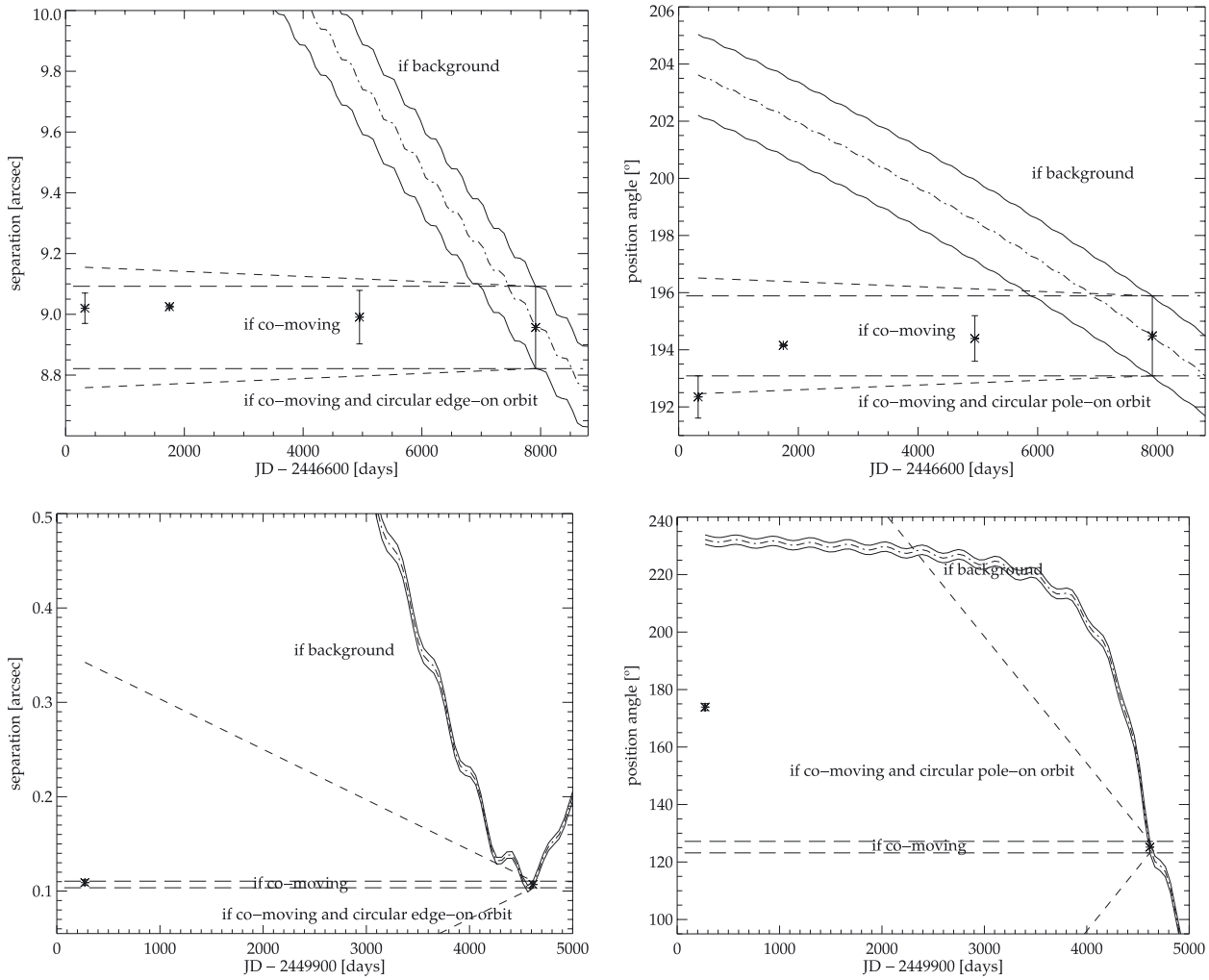

Fig. A.2. Proper motion diagrams (PMD) for separation and position angle change from absolute astrometric measurements of RX J0919.4-7738 B relative to the centroid of Aa & Ab (*top*, *left to right*) and from absolute astrometric measurements of RX J0919.4-7738 Aa relative to RX J0919.4-7738 Ab (*bottom*, *left to right*). See text for more information.

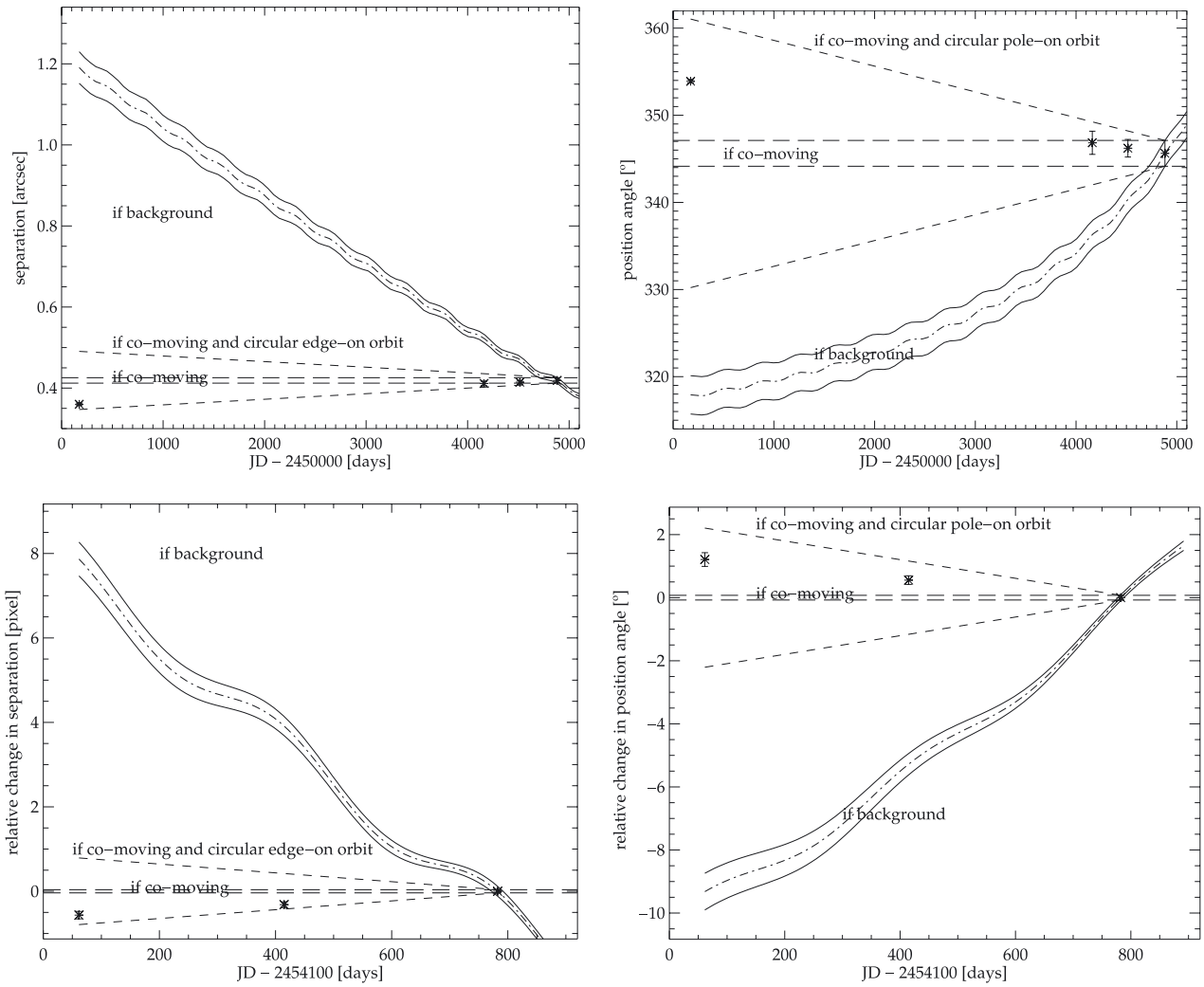

Fig. A.3. Proper motion diagrams (PMD) for separation and position angle change from absolute astrometric measurements (*top*, *left to right*) and from relative astrometric measurements (*bottom*, *left to right*) in the RX J0935.0-7804 AB system. See text for more information.

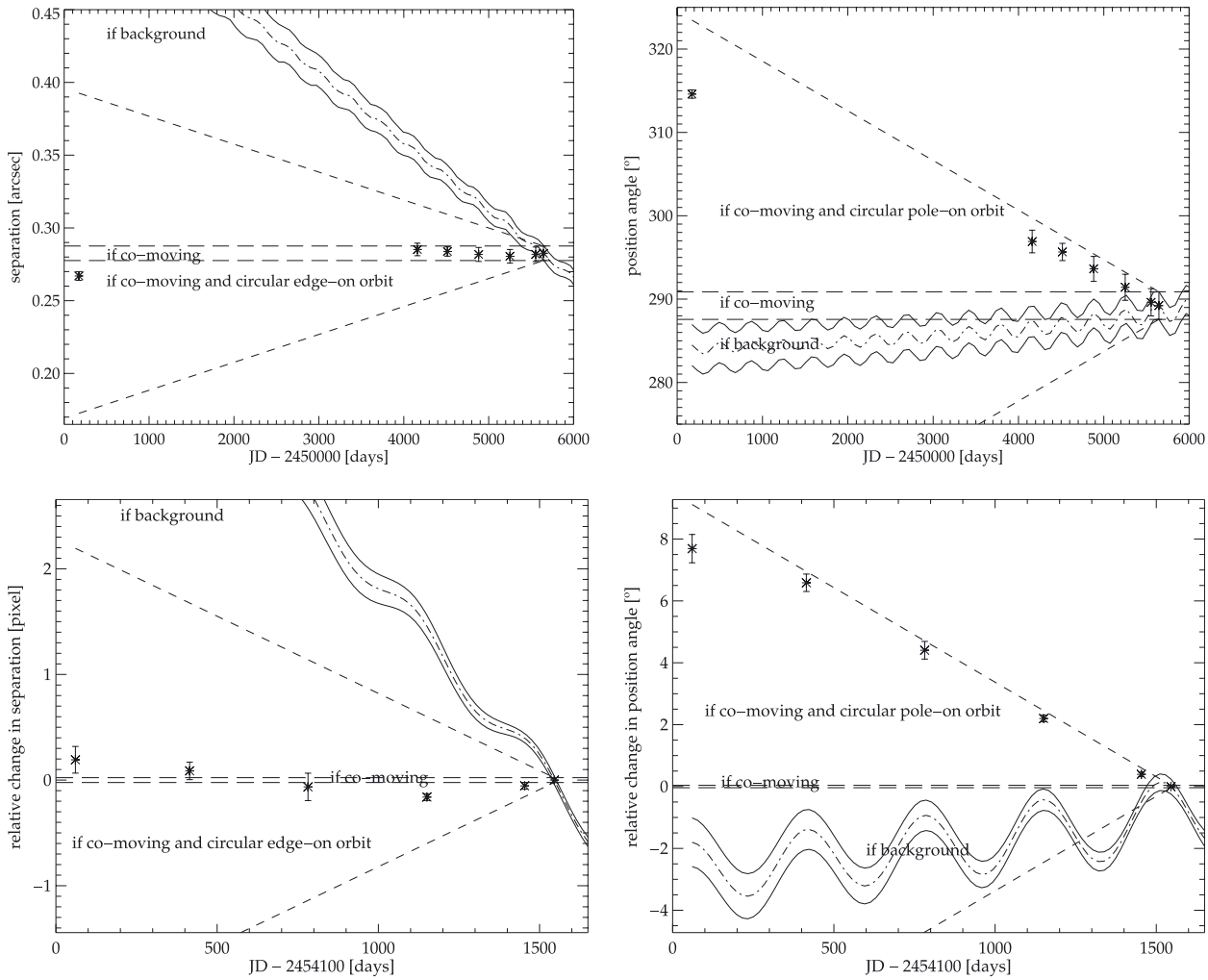

Fig. A.4. Proper motion diagrams (PMD) for separation and position angle change from absolute astrometric measurements (*top*, *left to right*) and from relative astrometric measurements (*bottom*, *left to right*) in the RX J0952.7-7933 AB system. See text for more information.

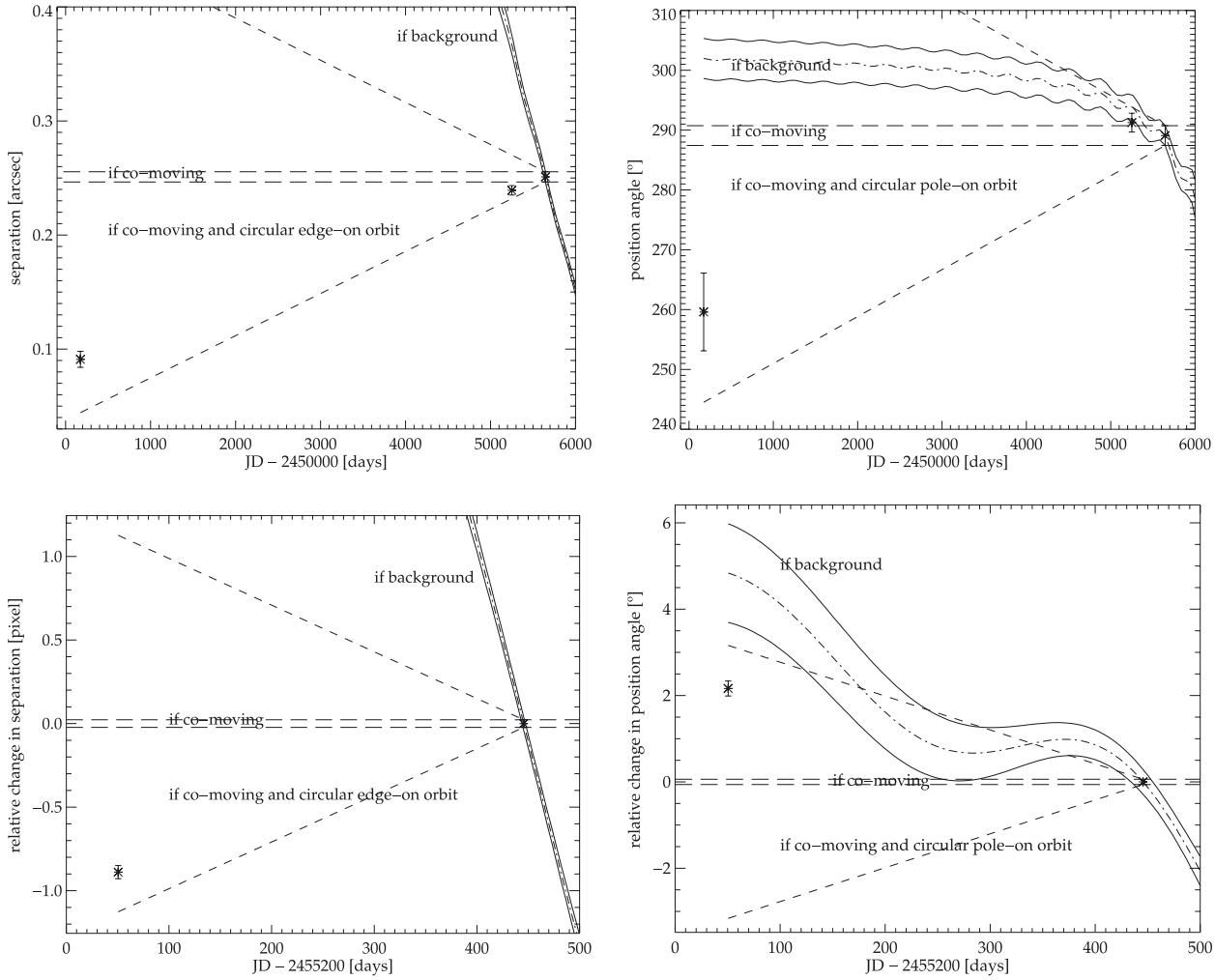

Fig. A.5. Proper motion diagrams (PMD) for separation and position angle change from absolute astrometric measurements (*top*, *left to right*) and from relative astrometric measurements (*bottom*, *left to right*) in the RX J1014.2-7636 AB system. See text for more information.

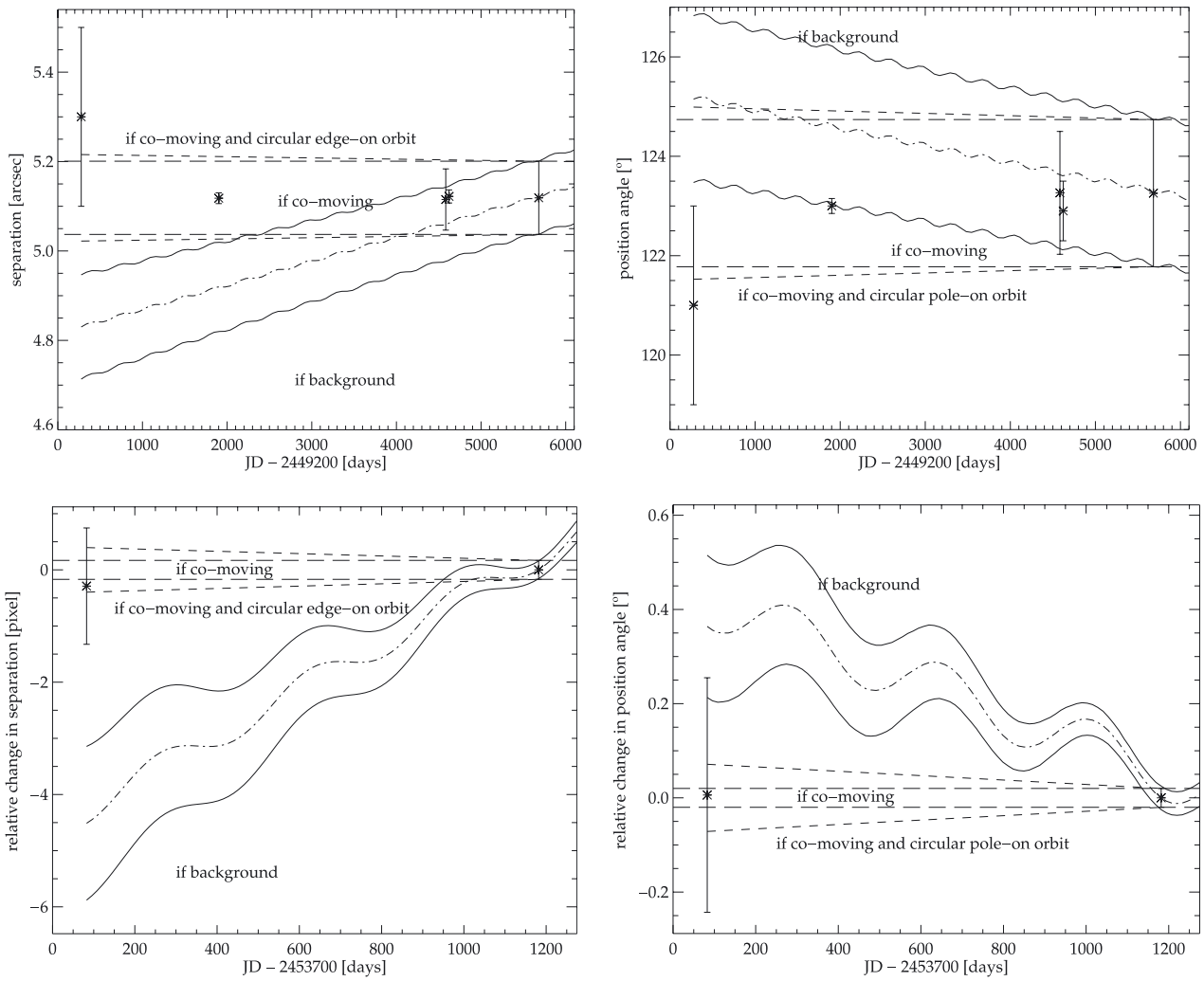

Fig. A.6. Proper motion diagrams (PMD) for separation and position angle change from absolute astrometric measurements (*top*, *left to right*) and from relative astrometric measurements (*bottom*, *left to right*) in the SZ Cha AB system. See text for more information.

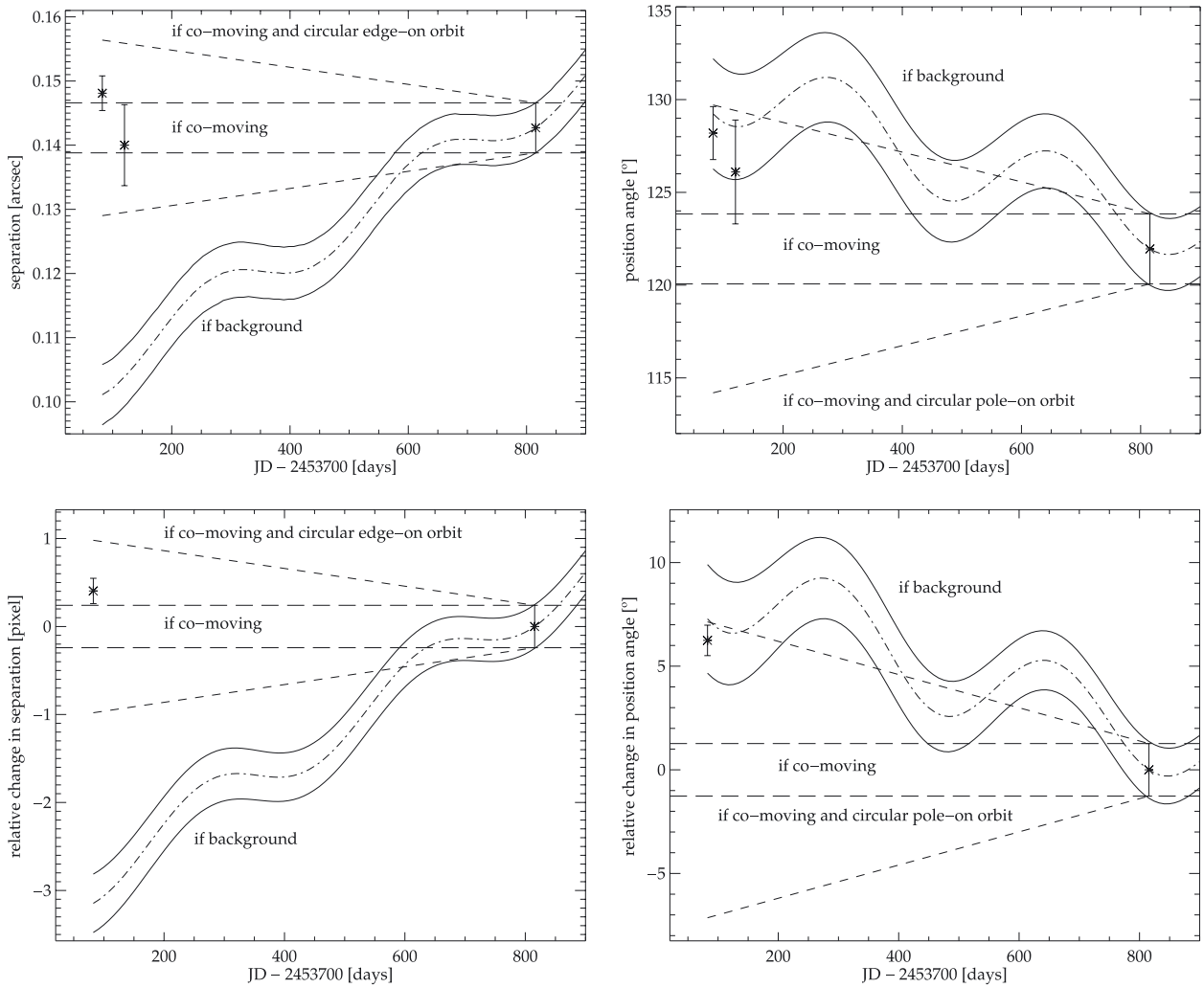

Fig. A.7. Proper motion diagrams (PMD) for separation and position angle change from absolute astrometric measurements (*top*, *left to right*) and from relative astrometric measurements (*bottom*, *left to right*) in the Ced 110 IRS 2 AB system. See text for more information.

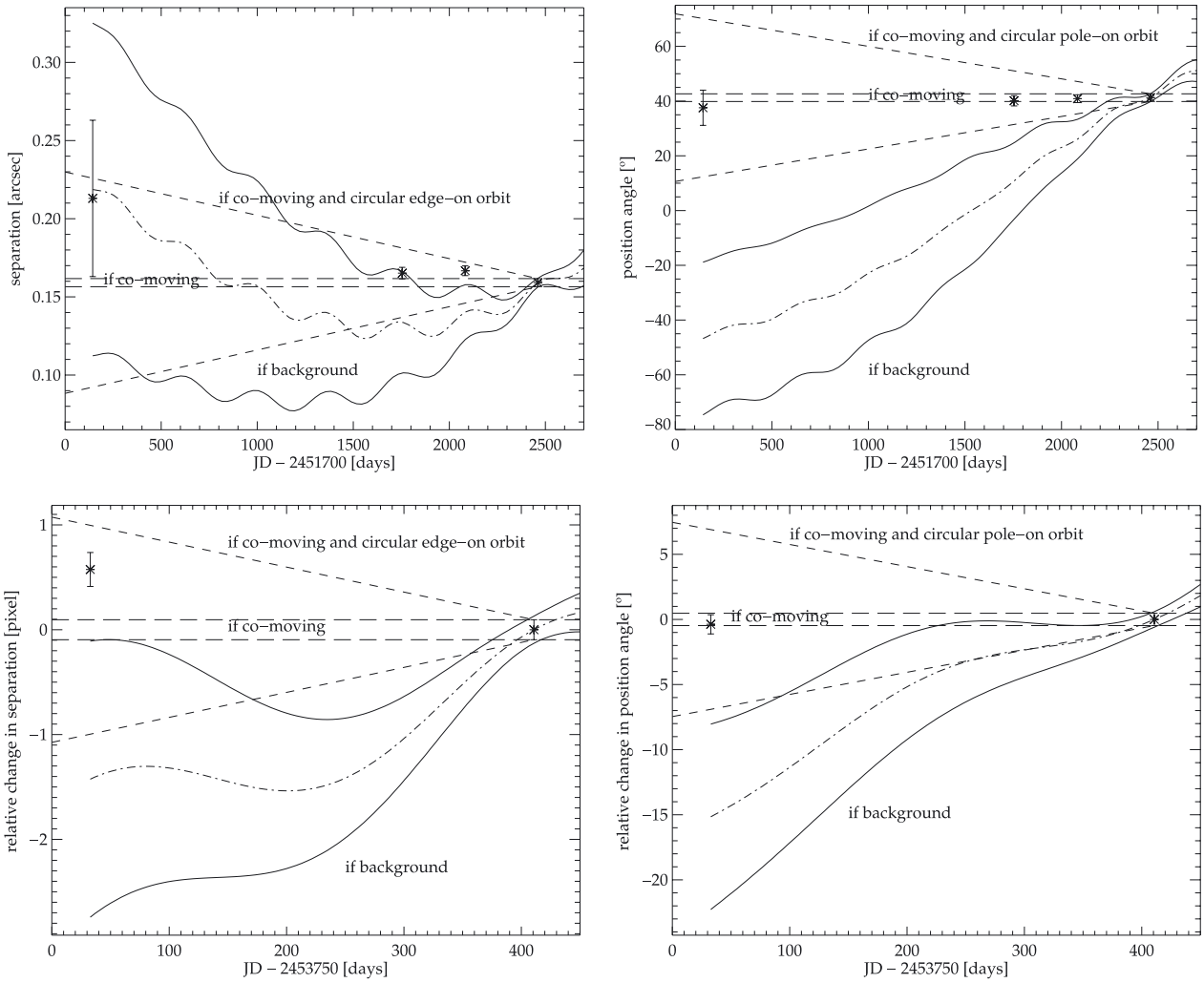

Fig. A.8. Proper motion diagrams (PMD) for separation and position angle change from absolute astrometric measurements (*top*, *left to right*) and from relative astrometric measurements (*bottom*, *left to right*) in the Cha Hα 2 AB system. See text for more information.

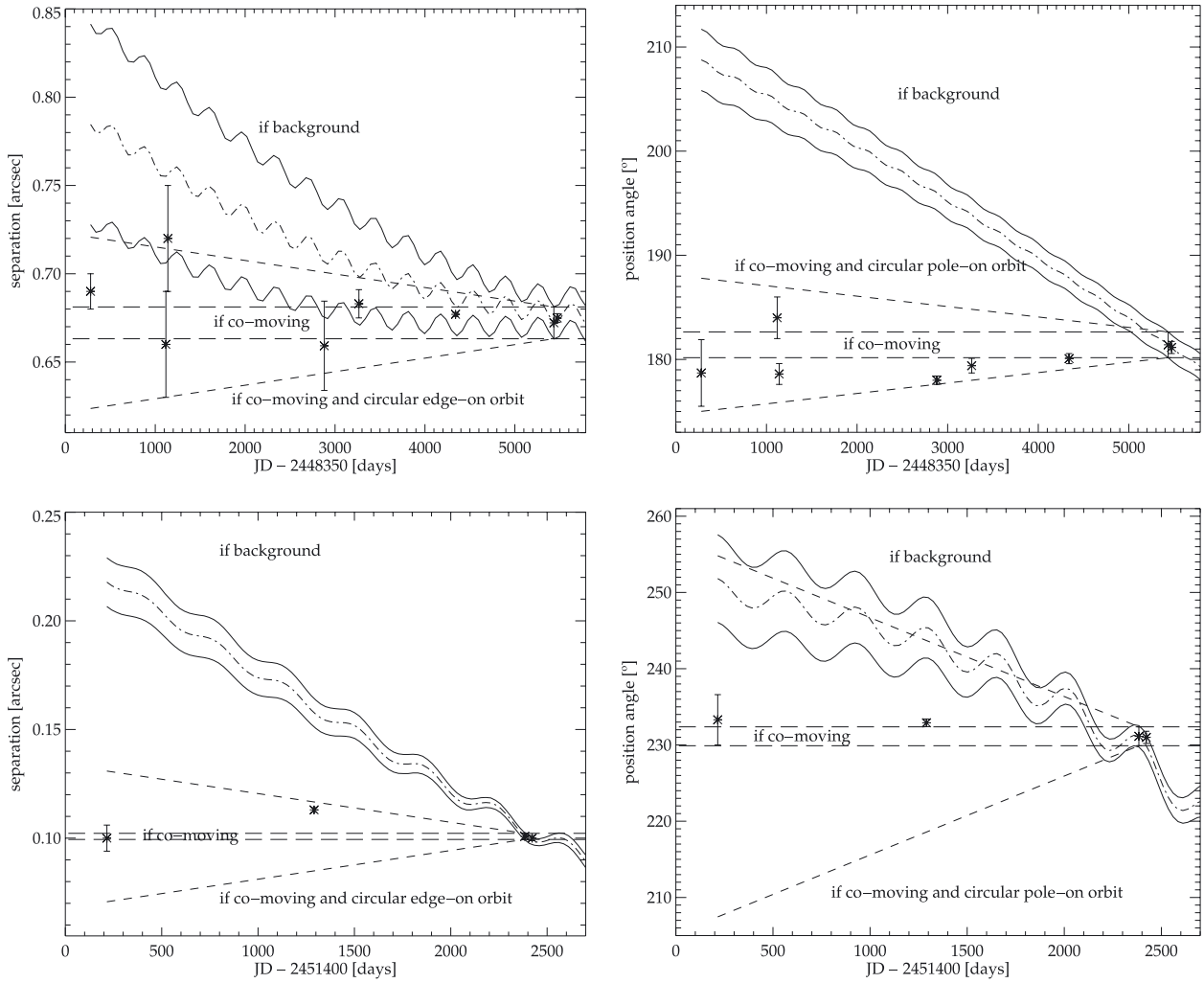

Fig. A.9. Proper motion diagrams (PMD) for separation and position angle change from absolute astrometric measurements of VW Cha A relative to the centroid of B & C (*top*, *left to right*) and from absolute astrometric measurements of VW Cha B relative to VW Cha C (*bottom*, *left to right*). See text for more information.

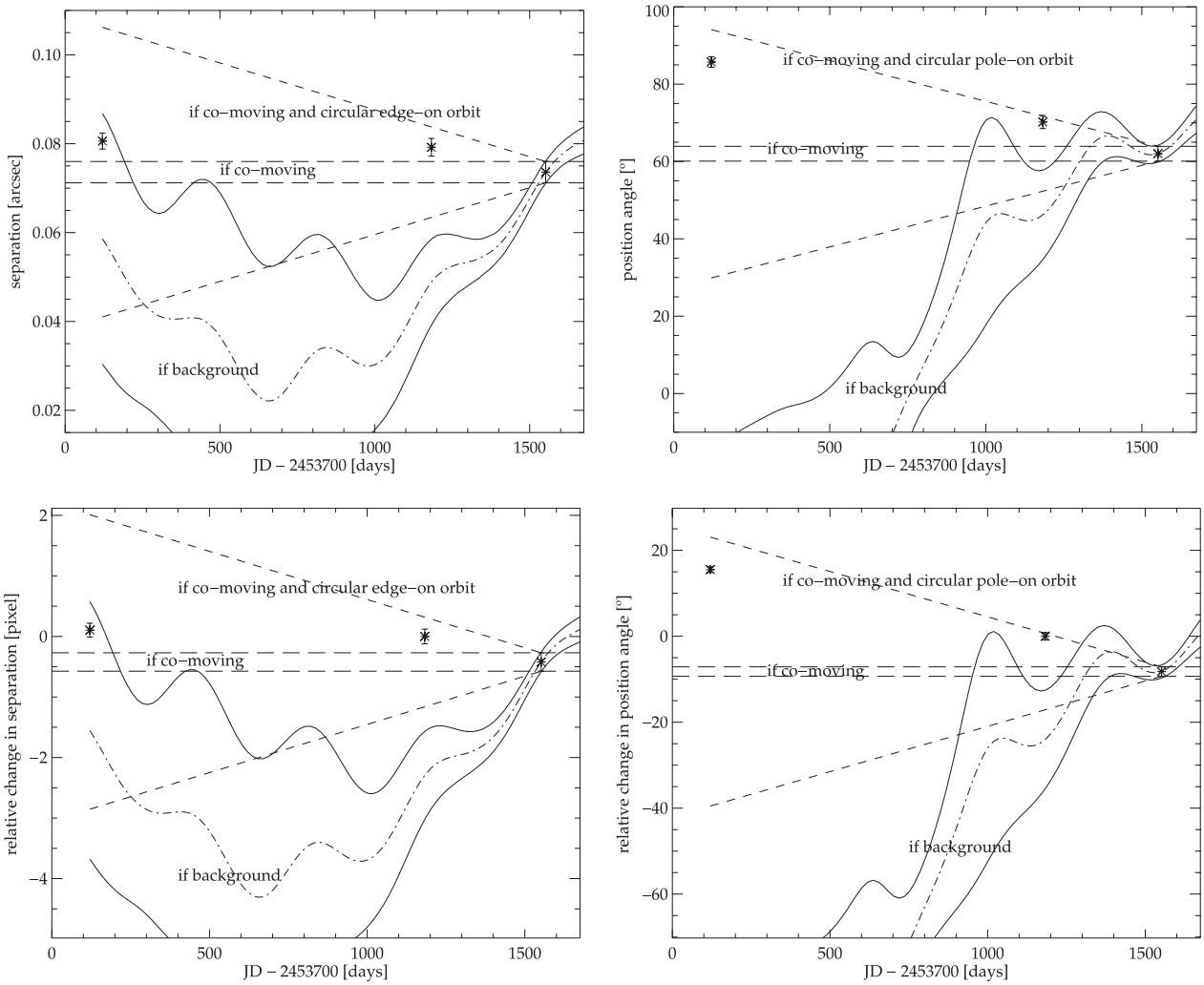

Fig. A.10. Proper motion diagrams (PMD) for separation and position angle change from absolute astrometric measurements (*top*, *left to right*) and from relative astrometric measurements (*bottom*, *left to right*) in the RX J1109.4-7627 AB system. See text for more information.

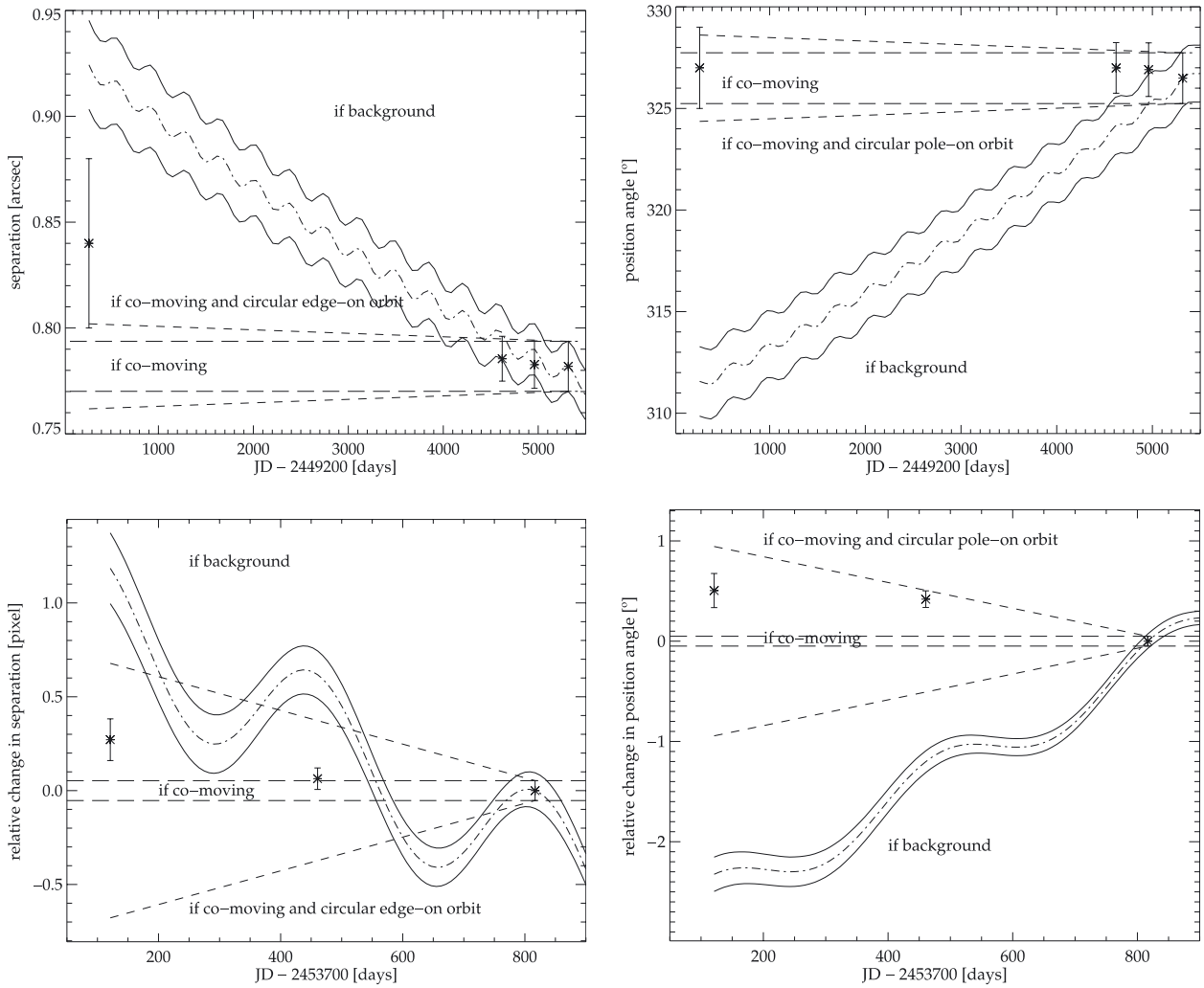

Fig. A.11. Proper motion diagrams (PMD) for separation and position angle change from absolute astrometric measurements (*top*, *left to right*) and from relative astrometric measurements (*bottom*, *left to right*) in the HD 97300 AB system. See text for more information.

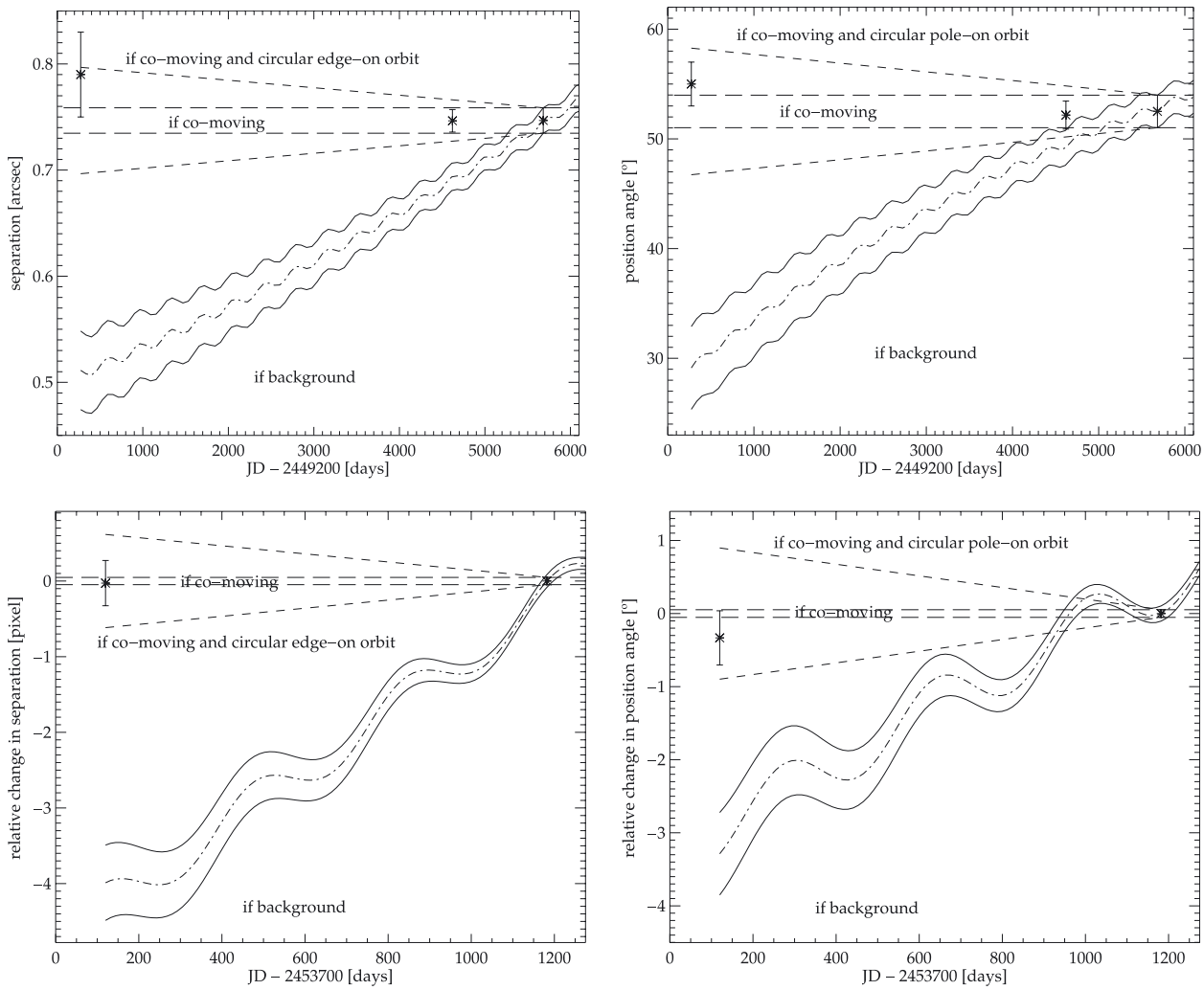

Fig. A.12. Proper motion diagrams (PMD) for separation and position angle change from absolute astrometric measurements (*top*, *left to right*) and from relative astrometric measurements (*bottom*, *left to right*) in the WX Cha AB system. See text for more information.

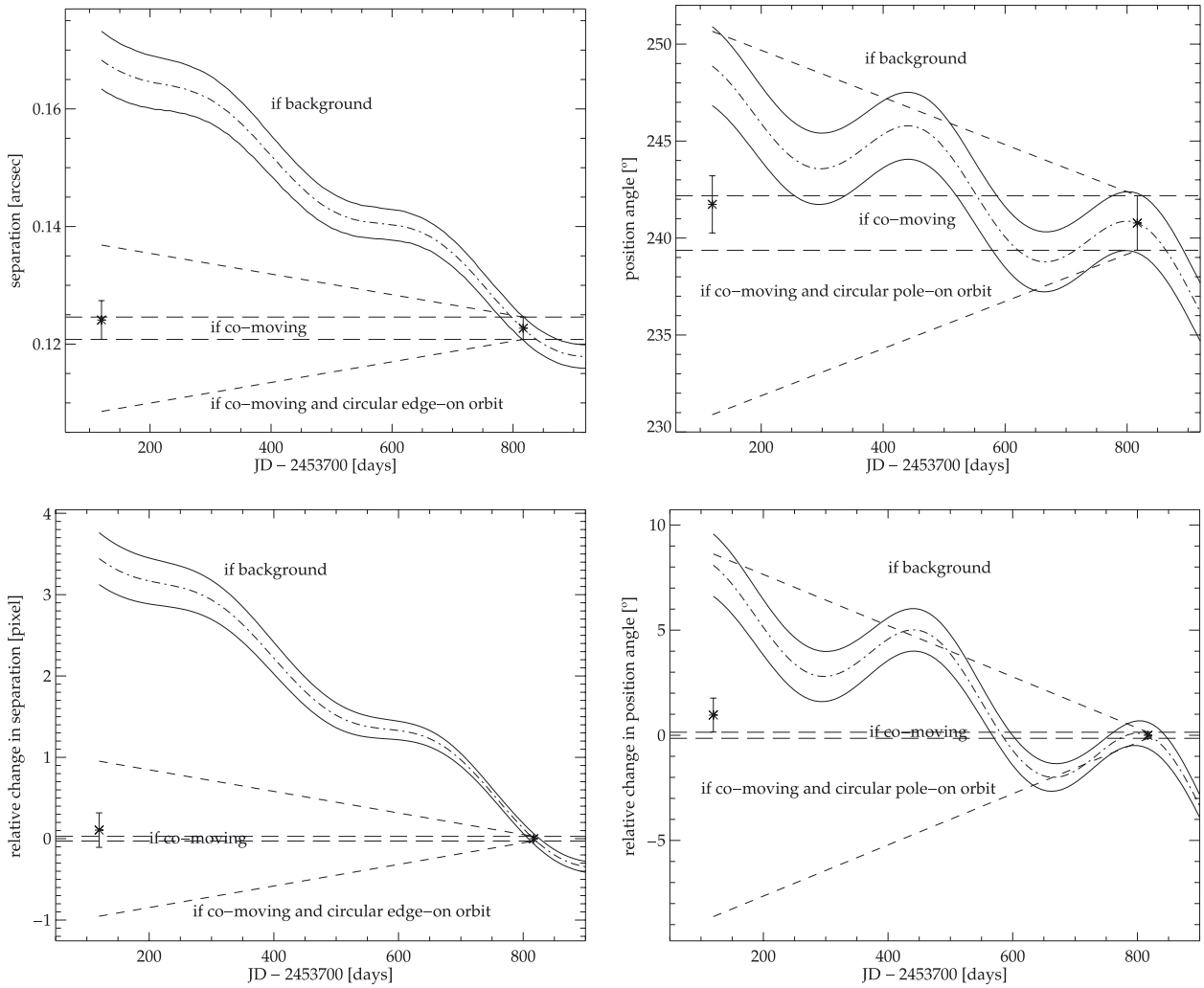

Fig. A.13. Proper motion diagrams (PMD) for separation and position angle change from absolute astrometric measurements (*top*, *left to right*) and from relative astrometric measurements (*bottom*, *left to right*) in the WY Cha AB system. See text for more information.

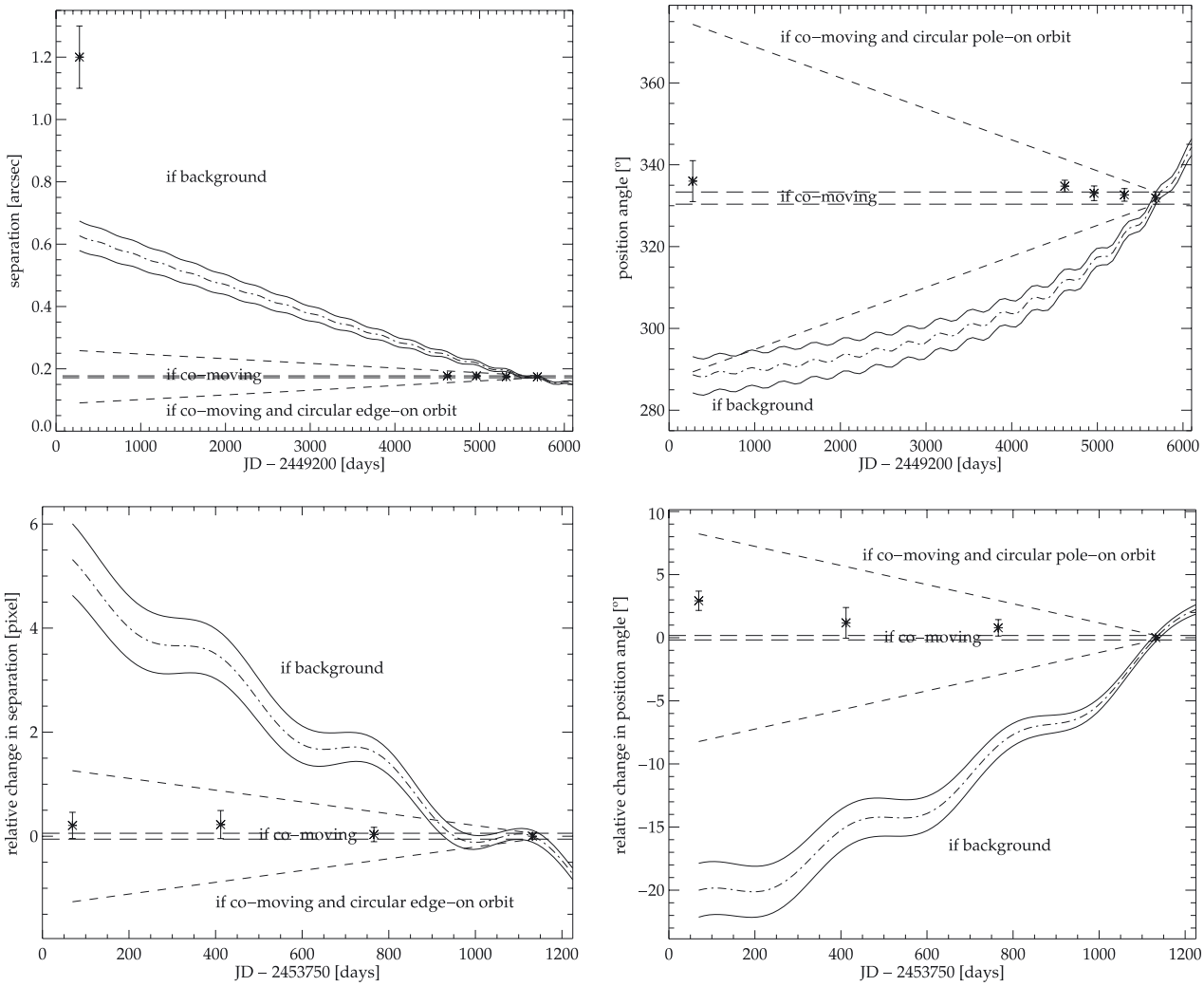

Fig. A.14. Proper motion diagrams (PMD) for separation and position angle change from absolute astrometric measurements (*top*, *left to right*) and from relative astrometric measurements (*bottom*, *left to right*) in the HJM C 7-11 AB system. See text for more information.

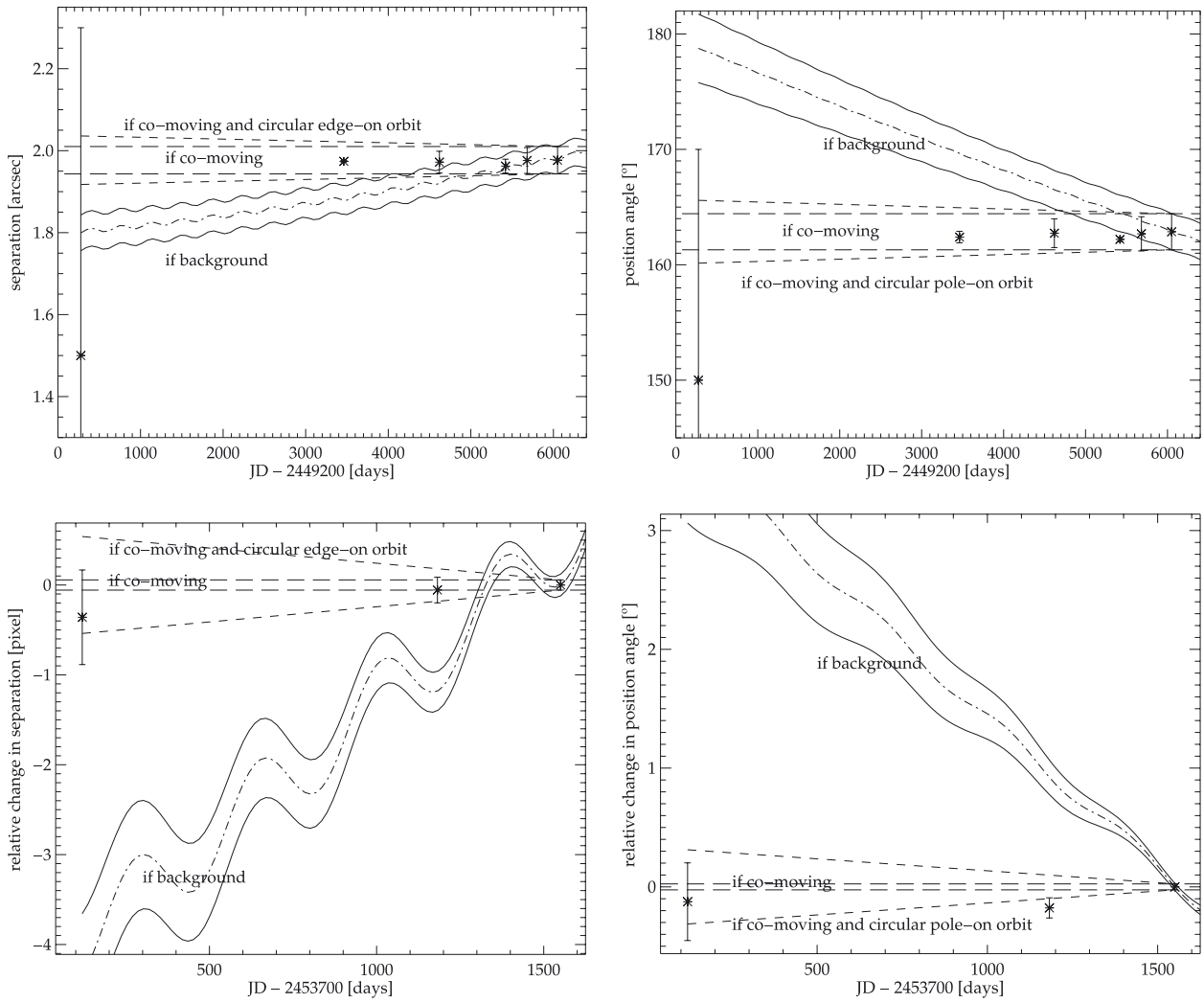

Fig. A.15. Proper motion diagrams (PMD) for separation and position angle change from absolute astrometric measurements (*top*, *left to right*) and from relative astrometric measurements (*bottom*, *left to right*) in the Sz 41 AB system. See text for more information.

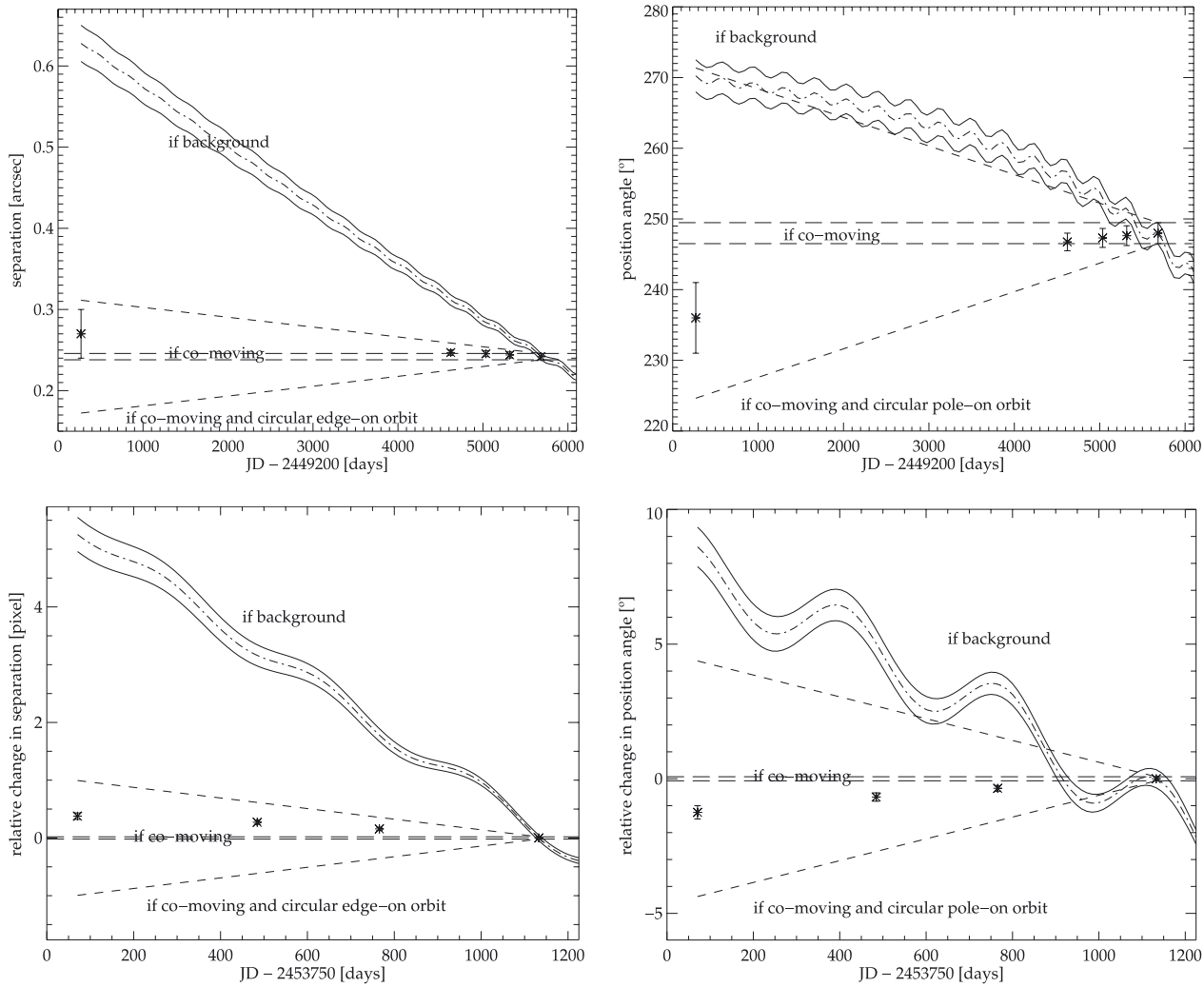

Fig. A.16. Proper motion diagrams (PMD) for separation and position angle change from absolute astrometric measurements (*top*, *left to right*) and from relative astrometric measurements (*bottom*, *left to right*) in the HM Anon AB system. See text for more information.